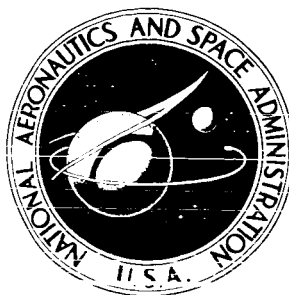


58 p.

**NASA CONTRACTOR  
REPORT**



**NASA CR-47**

**NASA CR-47**

N64-21420

0008-1 cat. 06

# **60-INCH STRETCH-FORMED ALUMINUM SOLAR CONCENTRATOR**

Prepared under Contract No. NAS 1-3216 by  
**THOMPSON RAMO WOOLDRIDGE, INC.**  
Cleveland, Ohio  
*for*

60-INCH STRETCH-FORMED  
ALUMINUM SOLAR CONCENTRATOR

This report was reproduced photographically from  
copy supplied by the contractor.

Prepared under Contract No. NAS 1-3216 by  
THOMPSON RAMO WOOLDRIDGE, INC.

Cleveland, Ohio

for

NATIONAL AERONAUTICS AND SPACE ADMINISTRATION

---

For sale by the Office of Technical Services, Department of Commerce,  
Washington, D.C. 20230 -- Price \$1.50

## TABLE OF CONTENTS

	<u>Page</u>
1.0 INTRODUCTION . . . . .	1
2.0 SUMMARY . . . . .	2
3.0 DISCUSSION . . . . .	3
3.1 Design . . . . .	3
3.1.1 Structural . . . . .	3
3.1.2 Thermal . . . . .	7
3.1.3 Concept . . . . .	10
3.2 Fabrication . . . . .	14
3.2.1 Facilities . . . . .	14
3.2.2 Tooling . . . . .	14
3.2.3 Stretch Forming . . . . .	19
3.2.4 Trimming . . . . .	22
3.2.5 Surface Improvement . . . . .	22
3.2.6 Reflective Coating . . . . .	26
3.2.7 Assembly - Shell . . . . .	29
3.2.8 Assembly - Torus . . . . .	38
3.2.9 Assembly - Concentrator . . . . .	38
3.3 Inspection . . . . .	39
3.3.1 Optical . . . . .	39
3.3.2 Weight . . . . .	46
3.4 Predicted Performance . . . . .	48
4.0 CONCLUSIONS AND RECOMMENDATIONS . . . . .	50

## LIST OF FIGURES

<u>Figure</u>		<u>Page</u>
1	MEMBRANE FORCES IN SHELLS	4
2	SHELL THICKNESS VS DIAMETER OR LOAD	6
3	SHELL AND TORUS TEMPERATURE PROFILES	8
4a	EFFECT OF TEMPERATURE CONTROL COATING	11
4b	TORUS SHIELD CONCEPT	11
5	60 INCH DIAMETER CONCENTRATOR - PHASE 2	12
6	CLEAN ROOM FACILITY	15
7	STRETCH FORMER AND TOOL	17
8	GLASS MASTER SURFACE RUN-OUT	18
9	SURFACE IMPROVEMENT SPRAY EQUIPMENT	24
10	REFLECTIVITY VS WAVELENGTH	28
11	ASSEMBLY AND INSPECTION RIG	30
12	INSPECTION OF 60 INCH CONCENTRATOR	31-33
13	SECTOR EDGE DISTORTION	36
14	60 INCH CONCENTRATOR - FRONT VIEW	40
15	60 INCH CONCENTRATOR - BACK VIEW	41
16	ABSOLUTE SURFACE ERRORS	43-44
17	X AND Y COMPONENT SURFACE ERRORS	45
18	TOOL, STRETCHED STOCK AND TRIMMED SECTOR ERRORS	47
19	EFFICIENCY VS CONCENTRATION RATIO	49

## LIST OF TABLES

	<u>Page</u>
I      BUFFER MATERIALS	20
II     PERTINENT CONCENTRATOR FACTS	27
III    ADHESIVES	37

## 1.0 INTRODUCTION

This final report discusses the work, results and conclusions on Contract NAS 1-3216 "60 Inch Diameter Stretch Formed Aluminum Solar Concentrator." The contract was performed under contract to NASA, Langley Research Center and extended over the period of June 24, 1963 to October 28, 1963 for delivery of a unit for evaluation. This contract is the second phase in the development of this concentrator concept and was preceded by the work on contract NAS 7-154. 21420

The objective of this contract has been to develop a solar concentrator made of aluminum, which will have performance sufficient for use in space power conversion systems. The design goal has been to achieve adequate surface quality for use in conversion systems with operating temperatures of 1800° Kelvin as are encountered in thermionic type devices. Such quality would also provide even higher performance in lower temperature applications such as the Rankine and Brayton cycle engines. The aluminum construction is desirable because of its lower specific gravity (with a resulting lower specific weight per power output ratio) and its non-magnetic property. AUTHOR

## 2.0 SUMMARY

All of the tasks in the contract work statement have been completed and a 60 inch solar concentrator has been delivered to the Langley Research Center for evaluation. By delivery of this report, the requirements of the contract will have been met.

Improvement in this phase 2 program has been demonstrated over phase 1 work. Of particular import was the 4 to 1 reduction of surface slope errors due to stretch forming. This improvement is basic to the number of available power conversion systems with which this concentrator concept may be used. In all other tasks, there were specific improvements. In the case of surface improvement coating the improvement was not as complete as desired. However, the task appears now to be somewhat more formidable a development effort than predicted. But the progress achieved on this program indicates that the desired results are near.

The conclusion then is that the stretch formed concentrator has been improved sufficiently to anticipate much more confidently its use with thermionic conversion systems. For other systems such as the Rankine or Brayton cycles, the concept is quite compatible and recommended. To further improve the surface coating process where the design can then be recommended for thermionic systems, a phase 3 program is recommended.

### 3.0 DISCUSSION

#### 3.1 Design

##### 3.1.1 Structural

The launch environment would cause the most severe loading of a concentrator. Since the concentrator shell is a membrane, the analysis is somewhat different than for a structure which has a high section modulus, such as honeycomb sandwich cross sections. For a membrane shell there can be a failure due to the material reaching its yield point or due to an instability or buckling condition. The mode of failure depends on the direction of loading. Inertia or pressure loads can either be applied as plus or minus  $p$  as in Figure 1. Here the inertia loads are treated as pressure loads. If the load is  $-p$  the membrane will fail by yielding. However, for the  $+p$  loads, the membrane can fail by buckling at some lower load than in the other case. Buckling failure in the shell is therefore not a function of the yield strength of the material but is a function of 1) modulus of elasticity, 2) specific gravity and 3) geometry.

Figure 1 shows the membrane forces which would exist in a paraboloidal or spherical shell for a given  $p$  load as long as the instability failure conditions have not been reached. Thus, the curves may be used for all  $+p$  loads up to instability failure and all  $-p$  loads up to the yield failure of the material. It should be noted that loads in either direction can be experienced due to vehicle acceleration (or deceleration), vibration, shock or acoustic noise. The curves show meridional and circumferential membrane forces for both paraboloids and spheres. With increase in edge angle, there is less agreement between the two solutions and paraboloids cannot be approximated by partial spheres. In fact, for angles of  $\theta$  greater than  $51^\circ 50'$ , circumferential stresses in the spherical shell change sign, whereas no such change occurs with a paraboloidal shells.

When buckling failure conditions are known to exist, the shell thickness must be sized by a buckling failure analysis. Minimum thickness to avoid buckling has been predicted by von Karman (Reference 1) and Reiss (Reference 2). For large ratios of radius of

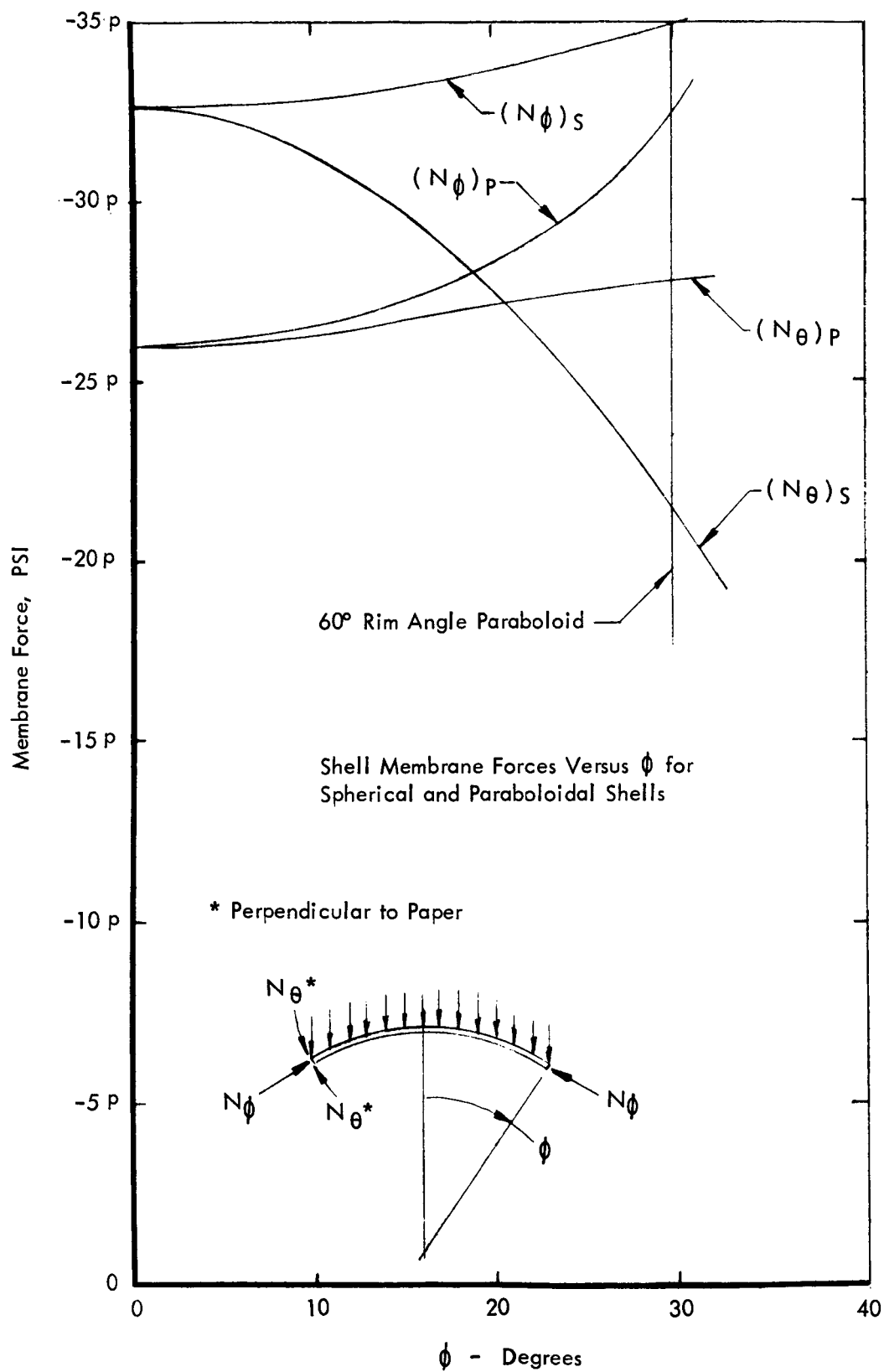


Figure 1

curvature to thickness, the Reiss criterion allows a buckling pressure 1/3 that for a complete sphere. It is, then,

$$p_{cr} = \frac{2 E h^2}{3 R^2 \sqrt{3(1 - \mu^2)}} = 900 h^2 \text{ (For Aluminum)}$$

For aluminum 60 inch concentrator shells and a given g load this reduces to:

$$h = .00011 g$$

The density of the material establishes the unit loading for a given g load, and therefore aluminum has definite weight advantages over other more dense materials. This comparison is shown in Figure 3.3-2, Reference 3.

Using aluminum, the curves in Figure 2 show 1) the minimum thickness to prevent buckling versus acceleration load for a 60 inch shell and 2) the thickness required to sustain a 10 g load for various shell diameters. For the present design where .016 inch aluminum stock is used, up to almost 150 g loads could be sustained. Thus thinner stock thicknesses may be used for less stringent conditions.

Elastic deflection of the shell during launch does not pose a problem since the unit is not performing at the time. This aspect need not be covered therefore. In the orbital thermal analysis (Section 3.1.2), it must be considered because the unit is operating.

The elastic and buckling failure analyses assume certain edge conditions on the shell. By separate analysis where the stiffness and cross section of the ring were considered, it was shown that a circular cross section torus attached directly to the shell provides the optimum design. This is particularly true if the mounts to the payload are limited to 3 as in this design. Without a rigid ring, the shell would deform considerably between mounting points. The difficulty in choosing the torus dimensions is therefore in maintaining sufficient rigidity while keeping the weight low. The 3" diameter, .025 inch thick torus cross section chosen for this design is considered conservative in this respect, and some weight reduction would be achieved with further analysis and experimental work.

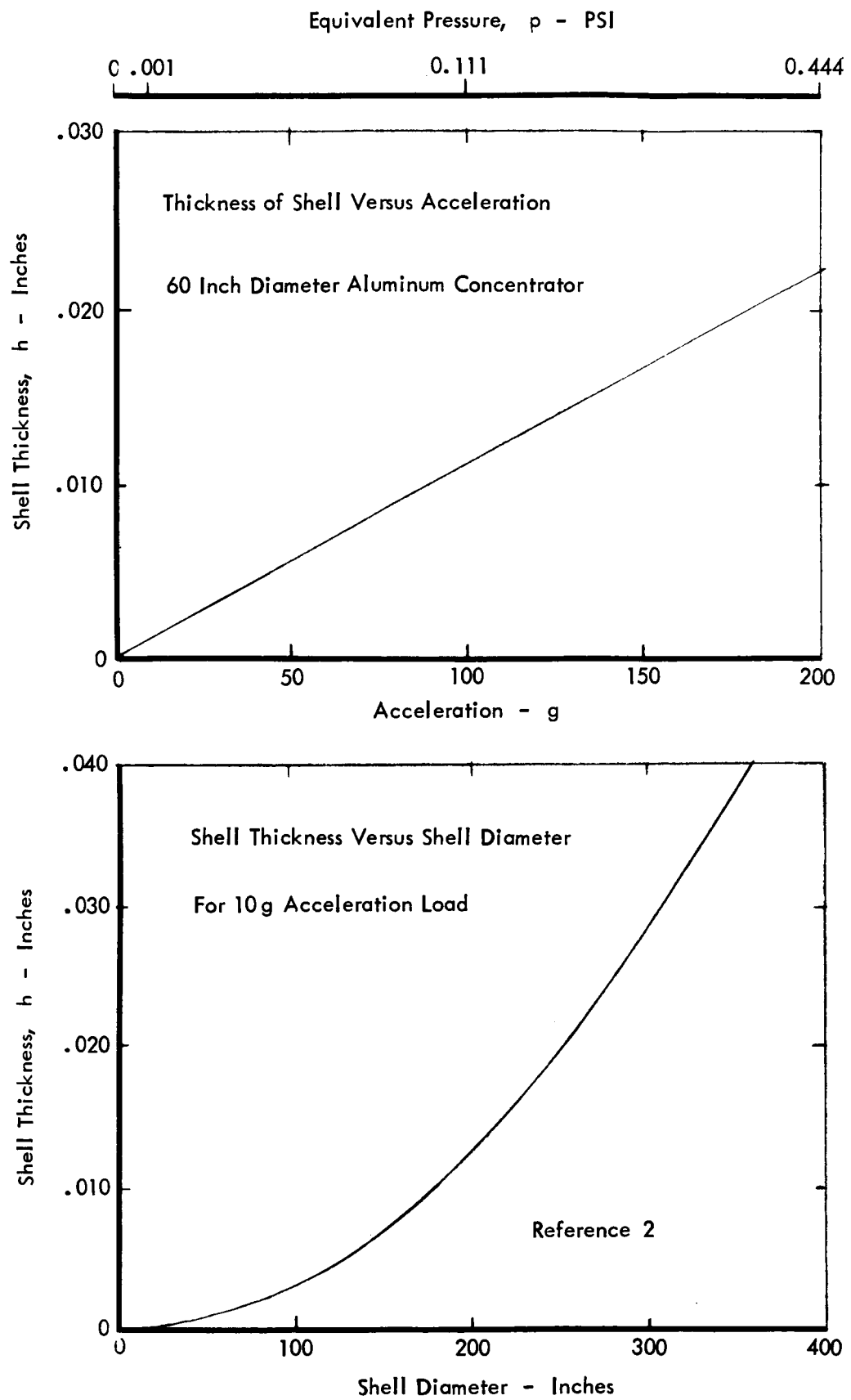


Figure 2

### 3.1.2 Thermal

A major point in the previous discussion on structural design was the conclusion to attach the shell directly to the torus without an intermediate section. However, the incident radiation conditions are drastic enough to require a detail analysis to determine whether this choice is thermally correct.

The 100 to 300 mile orbit conditions are more severe than the higher ones because of the effect of the widely varying Earth albedo and thermal radiation. Also, superimposing a 60 minute sun and 35 minute shade cycle causes step changes in the incident solar flux. Figure 3 shows incident flux intensity variations versus orbit time for a 300 mile orbit. An analysis to take into account the exact interchange of radiant conducted energy is beyond the scope of this program. However, it is felt that the simplification used in this analysis do not appreciably alter the first order effects. The transient temperature histories of the shell treated as an isothermal member and the torus treated isothermally were calculated, Figure 3. Of importance in these plots are the instantaneous temperature differences between shell and torus as each of the three cases are taken through an orbit period. Since the torus is the rigid member, any tendency for the shell to be at a higher or lower temperature level would be met by torus restraint and ultimate shell distortion.

Cases 1 and 2 treat the torus as isolated from the shell as regards conductive heat transfer. But the effect of being located on the sun side or shade side of the shell is observed. Case 3 is an approximation of the case where there is a highly conductive path from the shell to the torus. The curves of temperature versus time were obtained by taking small increments of time and calculating the time rate of temperature change:

$$\frac{\Delta T}{\Delta t} = \frac{q_i - q_o}{MC}$$

Some steady state points were also calculated at orbit positions of 1) just before emerging from the shade, 2) directly in line and between the Earth and sun and 3) just before entering

# SHELL AND TORUS TEMPERATURE PROFILES

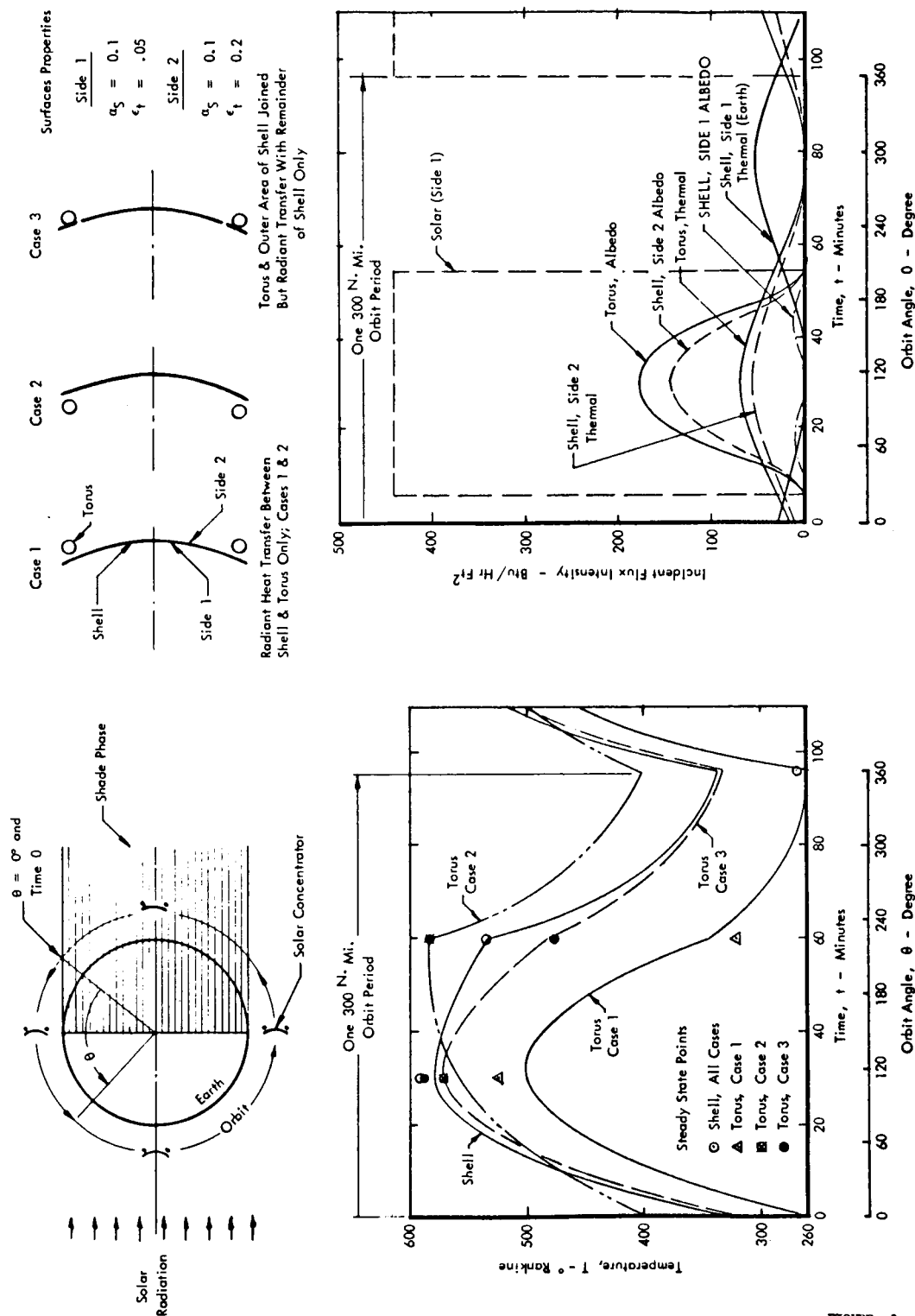


FIGURE 3

the shade again. In general the transient curve on emerging from the shade takes about 30 minutes to approach closely the steady state temperature. The transient curve on entering the shade never approaches the lower temperature level in the shade time span of 35 minutes.

Since the radiant transfer from shell to torus is significantly higher than from torus to shell, the shell temperature profile for all three cases would be about the same. However, the torus profiles vary one from another. For cases 1 and 3 the torus temperature is influenced largely by the shell heat input. In case 2 the sun also shows its influence wherein the temperature difference is positive and negative. Case 3 shows the least variation in shell and torus profiles over the sun phase. The maximum difference is about 50°F at the end of the sun period.

The effect of variation between shell and torus can be translated into equivalent loads and deflections. For a 50°F difference, the surface rotation at the outside edge of the shell is less than 4 minutes of arc and dampens out quickly. However, it should be pointed out that the assumption of no heat conduction between the outer edge and the remainder of the shell is unrealistic, but expedient for analysis. Actually, the heat in the shell would transfer to the torus as a sink and a lower gradient than calculated would exist. Thus the edge rotation would be reduced. The radial gradient caused by the heat flow to the torus requires some analysis to determine the degree of surface rotation. However, the direct attachment of the shell and torus appears to be the best method for least thermal effects. Thus the recommendation of the structural and thermal analyses is to fabricate the shell and torus together 1) without an intermediate member and 2) with a high heat conduction joint.

The surface thermal properties used in the analysis are listed in Figure 3 and were chosen because they are 1) characteristic of the usual surfaces to be used and 2) they do not involve temperature control surfaces which require additional processing or fabrication steps. However, after further analysis, it may be highly desirable that

special surface properties be utilized. As can be seen in all three transient cases, the temperatures cycle by about 200 - 250°F. Because of the wide range of cycling there can be more of a pronounced thermal lag between shell and torus, especially where the torus is dependent on shell temperatures. A non-gray coating exhibiting a low  $\alpha_s / \epsilon_t$  ratio is desirable here because it would have the effect of keeping the shade temperature higher. This is due to the higher absorptivity of Earth thermal radiation. Figure 4a shows the effect of using a thick silicon oxide (3 microns thick) layer, which exhibits such characteristics without significantly reducing reflectivity of solar wavelengths. The temperature fluctuation is reduced to about 60°F.

Another factor worth considering would be to more effectively control heat input to the torus. This could be accomplished by exposing a portion of the torus to solar input while shielding it from the Earth input. Figure 4b shows a concept which accomplishes this. The net effect would be to make the torus temperature less dependent on shell temperature (case 3) but prevent reversal of the temperature differential (case 2) due to higher earth input in the early and late stages of the sun phase. In general, the best solution to thermal distortion is to eliminate gradients rather than design around them by modifying shapes or building in additional restraint. It is still too early in thermal evaluation studies to determine whether special surfaces are required. Additional work is necessary for predicting and/or measuring thermal distortion effects.

### 3.1.3 Design Concept

Based on the previous analyses, the 60 inch concentrator design is as shown in Figure 5. The shell is still basically a membrane with no structural reinforcing and has not changed from the original concept (Reference 3). The significant design change is in the reinforcing ring cross-section and method of joining the shell and ring.

The basic torus cross-section was established at 3 inches diameter with a wall thickness of .025 inch. The attachment to the shell is direct without a cylindrical skirt, as in the previous units. This provides a good heat transfer path as well as a sufficient area

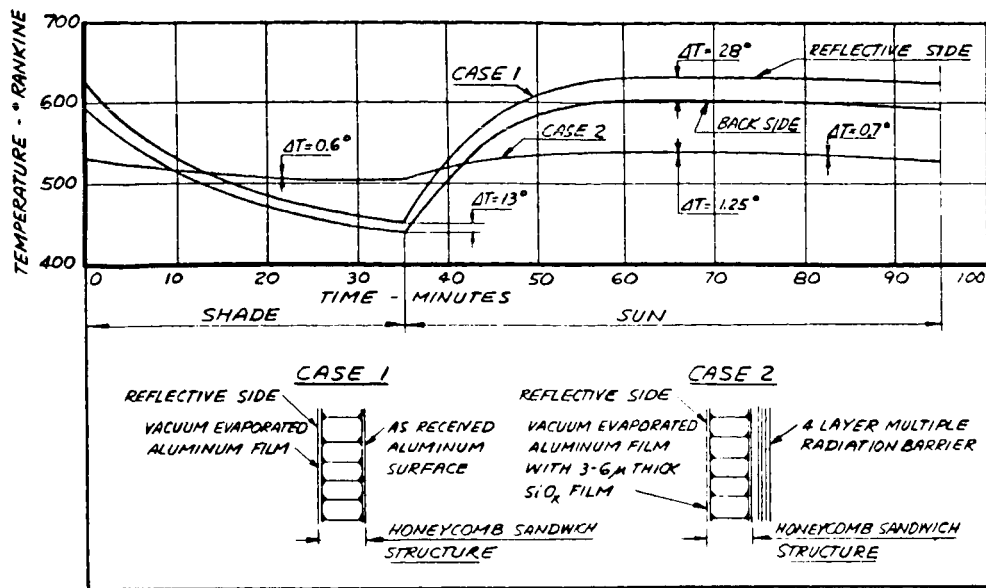
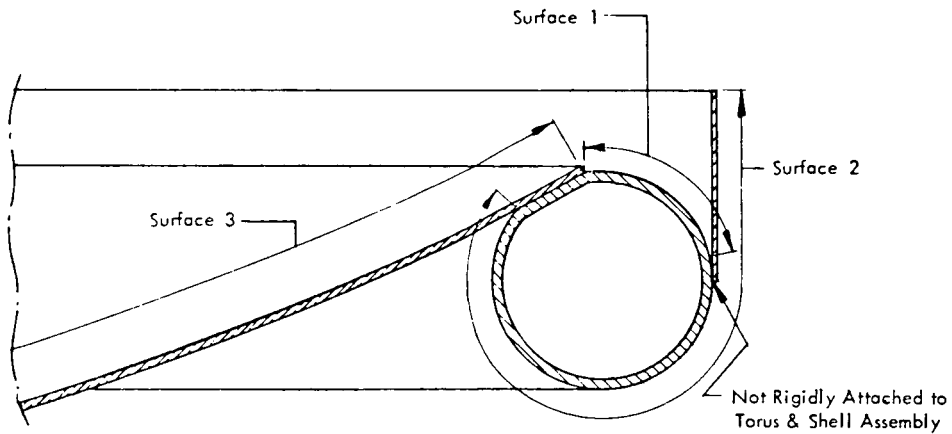


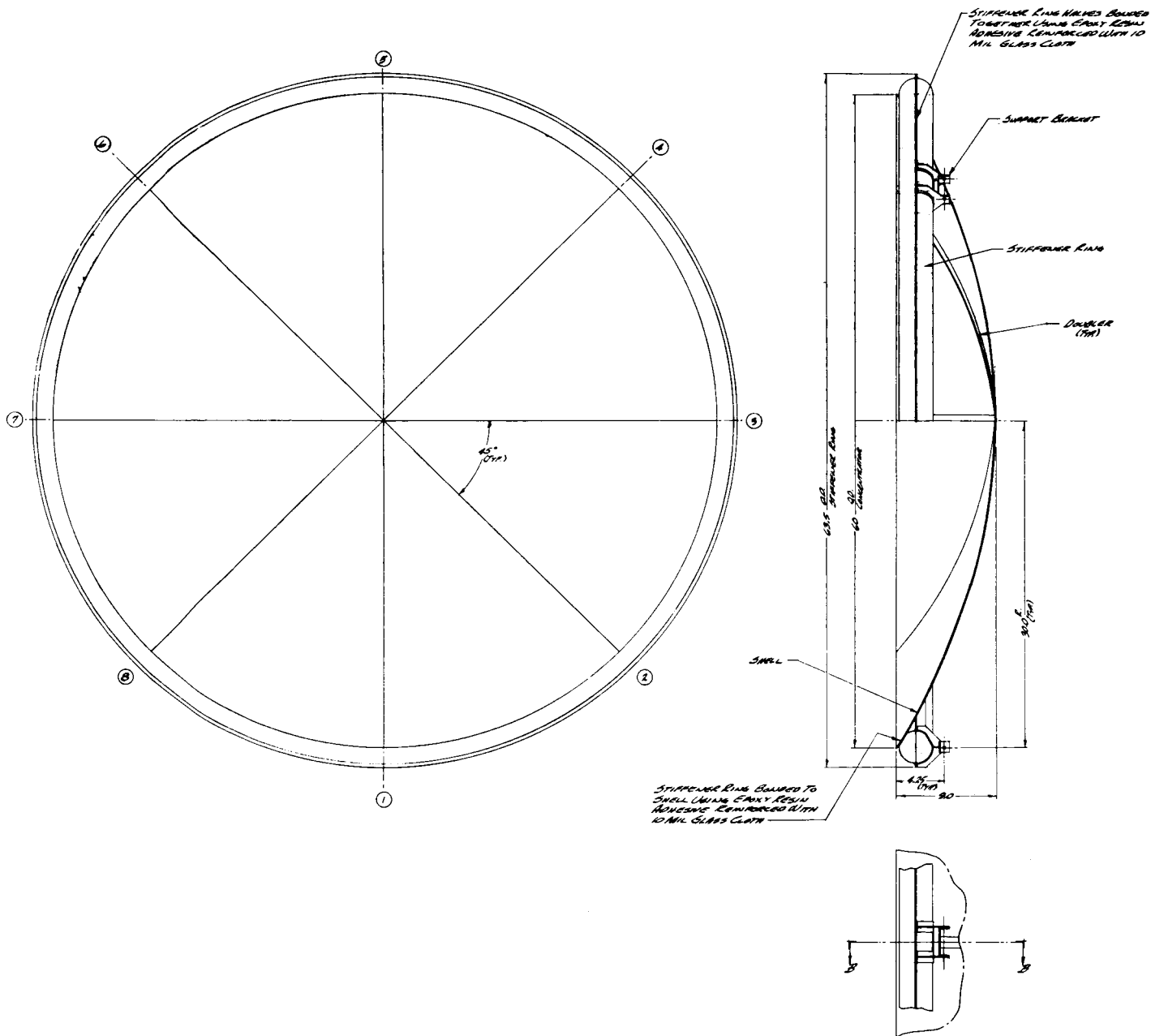
Figure 4a



#### Surface Thermal Properties

- Surface 1 -  $\alpha_s = 0.2$  to  $0.8$  (May Have a Matrix of Two or More Surfaces to Achieve a Specific Value)
- Surface 2 -  $E_t = .01$  to  $0.1$  (Multiple Radiation Barrier or High Reflectivity Film)
- Surface 3 -  $\alpha_s = 0.1$ ,  $E_t = 0.4$  to  $0.8$  (Silicon Oxide or Aluminum Oxide)

Figure 4b





of bond for transfer of shell loads to the torus. Thus a conical surface is formed into the toroidal section at the same 30° slope as the outside edge of the shell surface. See detail A, Figure 5.

The torus was formed in halves for two reasons 1) tubing of 3 inch OD x .025 wall is not available and 2) the torus can be made to match the shell shape. This latter point requires further explanation as follows. The torus by itself has considerably more rigidity than the shell by itself. Thus if the formed torus has waviness in a true-indicator scan of the conical mating surface, the shell will be forced to take a distorted shape. This run-out would be anticipated in rolling of tubular sections. Therefore the fabrication procedure using two torus halves is as follows:

1. Place 8 shell sectors on aligned master, join radial gaps and cure.
2. Place one torus-half on shell, with no adhesive between shell and torus-half.
3. Apply adhesive to the inner and outer torus-half lips.
4. Place second torus-half on first torus-half.
5. Apply a uniform load on the second torus-half during the torus cure cycle to assure good lip bond and conformance of the torus to the shell shape.
6. When torus halves have cured together, place adhesive between shell and torus and cure. This cure does not require loading the torus except for a minimum required to cause void filling by the adhesive.

Because of the change in ring design, the three mounting brackets were modified. The centerlines of the three .3125" diameter mounting pin holes are still tangent to a 60 inch diameter circle, however. Attachment of the bracket assembly to the torus is by adhesive bonding but with supplemental rivets to secure the bracket during curing.

The shell material is of 3003-0 aluminum alloy instead of 5052-0 as in the phase 1 units. This alloy has superior plastic strain properties where there are no gross surface distortions due to non-uniform strain and the resultant exhibition of Lueder's lines.

## 3.2 Fabrication

### 3.2.1 Facilities

One of the problems encountered during fabrication of the previous phase 1 units was room cleanliness. Both the stretch forming and surface epoxy coating sequences were sensitive to particles in the air. This resulted in surface imperfections that cause performance degradation. Therefore a clean facility was considered necessary. For this phase 2 program, a dormant clean facility, Figure 6, was located within the division. All of the fabrication (except trimming and vacuum metallizing) and the optical inspection are now performed in this room. The air is filtered, temperature controlled to  $\pm 1/2$  °F and humidity controlled to 40% RH.

The stretch forming, spray coating and optical inspection equipment were modified to major extent and will be discussed in the following sections.

### 3.2.2 Tooling

The epoxy replica tool used in the phase 1 program had known surface errors which did not exist on the glass searchlight mirror original. The errors occurred during the female pattern fabrication, and funds did not allow correction. For this phase the glass master itself was used for forming, thereby eliminating errors which could occur in the two surface replications required. The unit loads due to forming are low and cause compressive stresses which glass can withstand most readily. A poorer glass master was tried first however to assure that the good master would not be cracked.

The old tool was used as the underframe for the glass, although an intermediate layer of hydracal was used to assure that the glass was in alignment. The master was silver coated on the convex side (same side as used for stretching and assembly) and supported at six points on the edge while in the inspection rig. The mirror was aligned until the best projected grid pattern was obtained. Then the space between master and floor was filled with sand and the pattern re-checked. There was insignificant shape change.



CLEAN ROOM PRIOR TO MODIFICATIONS

Figure 6

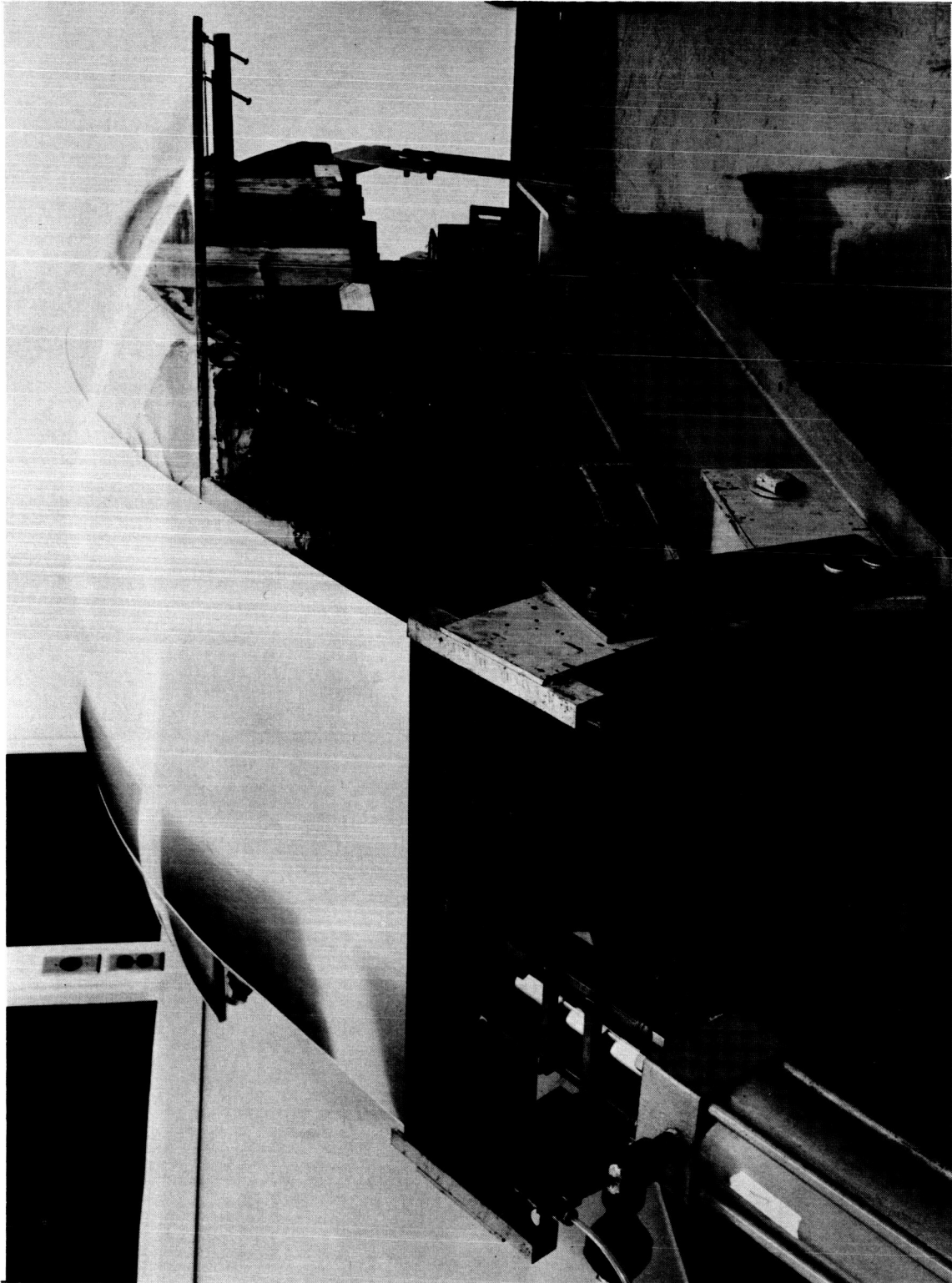
The sand was used to prevent deflection or cracking of the master under loading by the hydracal and underframe. The underframe was placed over the master with a gap between them. The gap was then filled with hydracal and allowed to set. Since the same master must be used for assembly of the concentrator, a separation layer was used between the master and hydracal.

The master and underframe were then turned over and positioned in the clean room as shown in Figure 7. Since the master over hung the underframe edges, it was necessary to put adjustable supports at two points on each side. The master was adjusted on the tool and inspected with a dial indicator (Figure 3.9-3; Reference 3). Figure 8 shows the run-out at various circumferential lines on the master. Maximum surface slope errors of only 0.9 minute were measured. This indicated that the master did not shift during pouring of the hydracal and that an accurate forming tool was achieved.

It should be noted that some preliminary work was performed in selecting the best master for the program and the best method of making an accurate tool. Two glass masters were optically inspected and the one used had errors of one magnitude less than the other. The poor master showed some areas where 30 minute errors existed. As was shown in circumferential measurements, the good master is far superior.

The masters were also studied under three methods of support: 1) concave side up and uniformly supported with sand, 2) concave side up and at six points at the edge and 3) convex side up and at six points at the edge. It was concluded that all three support methods resulted in an insignificant change (for the application) in shape of the master surface. Thus, the master is relatively stiff and distortion-free under these support conditions. However, it was relatively easy to adjust at the six points until the optimum shape was attained.

Based on these results it was also decided to use a new method of assembling the collector while in the optical inspection rig. This will be described in section 3.2.7.



STRETCH FORMING MACHINE WITH STOCK IN STRETCHED CONDITION

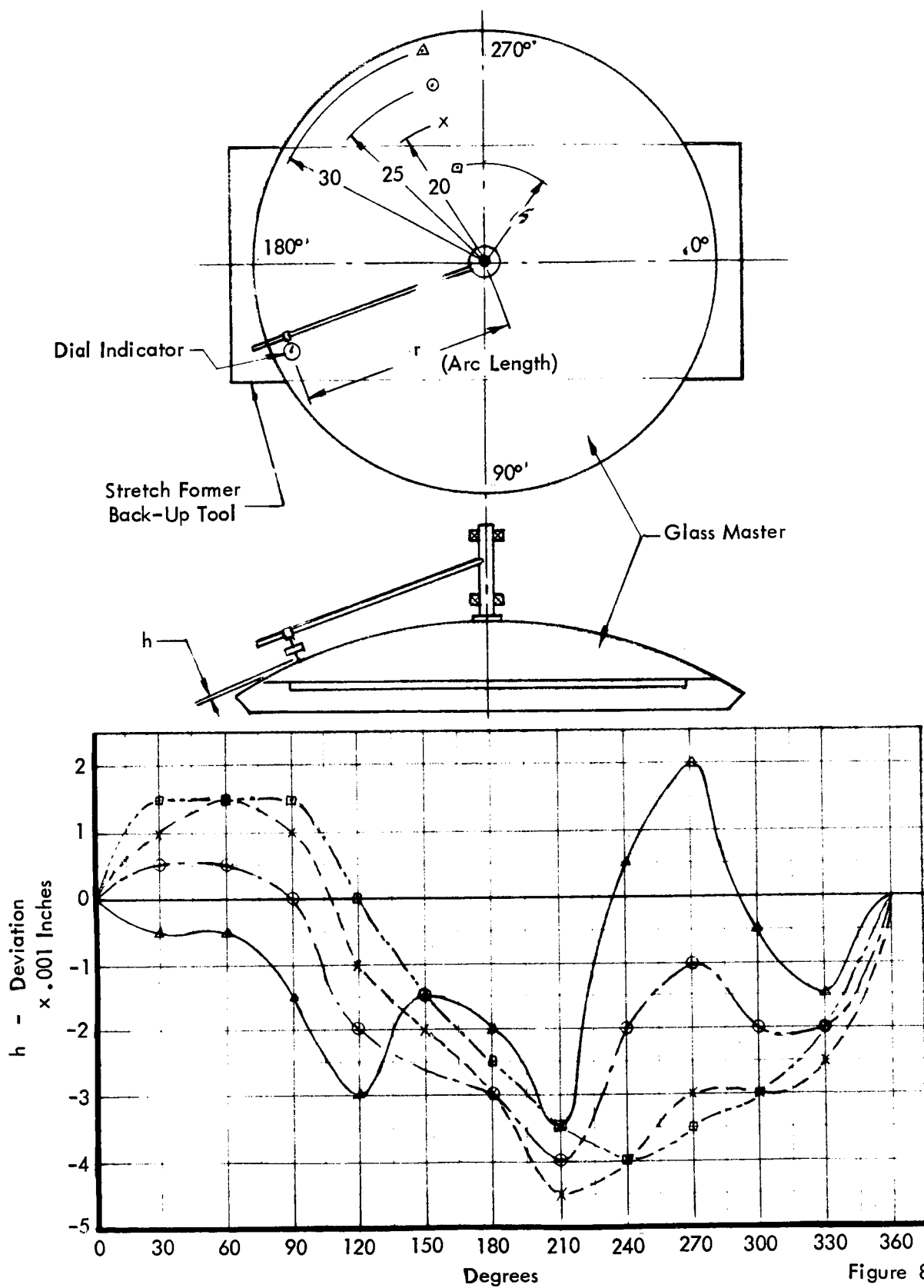


Figure 8

### 3.2.3 Stretch Forming

The stretch forming machine is shown in Figure 7 with stock in the full stretched condition. Modifications were made to the machine including 1) improved jaws, 2) improved hydraulic plumbing and 3) new stretch limiters on the jaws. A transition apron on either end of the tool was added to prevent edge loading of the master.

A new lot of aluminum alloy 3003-0 was ordered to replace the 5052-0 supply, which formed undesirable strain lines. The stock was supposed to be .016" but measured closer to .017", although of uniform thickness. The rolled surface finish was within specification (estimated less than 2 microinches RMS maximum), but the 3003-0 stock is softer and had "eyebrows" due to handling at the mill. These "eyebrows" remain as elongated defects after stretching, but they can be eliminated by proper handling at the mill. No additional "eyebrows" were formed during handling at TRW.

The stock was stretched 4% along the center of the panel and 2% along the edges. Upon release of the jaw pressure, a small jaw return occurred which is explained by the elastic return down the stress-strain curve. Except at the very edge, there was no indication of voids or spring-back when the stock was finger tapped.

Selection of a buffer material between the tool and stock was a major effort and caused some delays. Emphasis was placed on liquid lubricants, especially the more recent promising developments. Some of the products were more of a grease and grease suspension type. Those evaluated are listed in Table I. Initial stretching was performed on the master with the silver inspection layer in place. The layer thickness was only microinches thick, and its retention was needed in eventual master alignment in the assembly rig. However, an undesirable action occurred when liquid oils were used. The oil caused troughing due to non-uniform application. When the oil layer was reduced to eliminate non-uniformity effects, the layer was too thin and scratches were noted. These scratches were due to contaminants in the oil, primarily due to personnel handling the stock.

TABLE I  
BUFFER MATERIALS

No.	Compound	Type	Manufacturer
1	S-122 Fluorocarbon	Spray on Dry Film	Miller-Stephenson
2	Poxylube 420	Spray on Dry Film	Poxylube
3	22-T	Spray on Dry Film	Electrofilm
4	Cindol 3103	Liquid	E. F. Houghton
5	#40 Drawing Comp.	Liquid	Chandler Chem.
6	Product 1450	Liquid	Lubriplate
7	Dietone A	Liquid	Kondok Prod.
8	Alco #3X	Liquid	Rex Oil
9	813A	Liquid	Murphy-Phoenix
10	813B	Liquid	Murphy-Phoenix
11	813C	Liquid	Murphy-Phoenix
12	K-25	Liquid	Murphy-Phoenix
13	EX-968	Liquid- Strippable	3 M Co.

The next step taken was to stretch dry with personnel wearing clean uniforms, hats and boots. Wet lint-free sheets were hung to reduce particle content in the air. Scratching was still observed and became worse with each stretched panel. When it was noted that some scratch patterns repeated, the silver surface was observed under magnification. It was found that lack of lubricant was causing local adhesion of the aluminum to the silver and even bare glass where silver was stripped. The adhesion to the master caused repeated adhesion frequency in subsequent stretches. Thus the master was stripped of silver, except for 6 reference spots outside the trim area used for eventual alignment in the assembly rig. The aluminum particles were then removed also.

To eliminate further aluminum adhesion and to avoid dirt contamination, a spray-on dry fluorocarbon lubricant was used. This provided the final solution to scratch free and trough free stretched panels. However, the spray lubricant occasionally spurts small particles which were removed where possible. To eliminate particles from the air, the stock and tool were air sprayed and the stock quickly placed over the tool. Just prior to stretching, the gap between stock and tool was again air washed. Personnel wore clean clothing, but wet sheets were not considered necessary. Some additional refinements can be made, but the stretch forming techniques are quite adequate.

A total of 19 sheets were stretched, and the last 8 were used to select 8 sectors for the concentrator assembly. Each stretched sheet provides 2 trimmed sectors. There was no significant difference in surface quality between sectors stretched over one side as compared with the other side of the master. In the final assembly, the ratio was 5 sectors from one side to 3 from the other.

As shown in optical inspections, the stretched panels have good surface conformance to the tool. This is shown later in the discussion on the assembly inspection. The stock did not exhibit Lueders lines and strained very uniformly. The surface finish does change, however, from a lustrous to a fine grainy surface due to grain reorientation

and slippage. The finish is estimated to be less than 10 microinches RMS maximum and is not of the quality required for concentrator surfaces. This necessitates the use of surface improvement coatings (to be discussed later).

#### 3.2.4 Trimming

The sectors were trimmed with a high speed slitting saw as in previous units (Reference 3), and there were no requirements for changes in the trimming techniques for this phase 2 work.

#### 3.2.5 Surface Improvement

A surface improvement coating is necessary in the stretch formed aluminum fabrication process. Such minute imperfections as strain graininess and occasional scratches cause a high diffuse component in reflected light.

But the depth of surface deviation is small enough to allow use of a surface coating, which results in a "varnish" action wherein the resulting surface is mirror-like in finish. An epoxy is used because of its anticipated resistance to space environmental effects. However, the formulation and application of these thinned epoxies was not adequately resolved in the phase 1 units.

The second and third units in the phase 1 program were made with sectors that were dip coated. Spray coating was preferred, but equipment capable of uniform application was not available and funds prevented purchase. Dip coating resulted in formation of "record grooves" and non-uniform layer thickness. The grooves formed in the direction of run-off. Thus, it was determined that a spray-on technique should result in an improved surface layer.

Vendors were contacted regarding both air and air-less spray equipment. It was determined that an air type spray system was preferable, even though air atomization might cause considerable overspray. In air-less systems it is necessary to pressurize the

liquid to high pressures of 500 to 2000 psi which has been noted to cause some polymers to partially cure with a resulting subgrade coating.

In addition to the spray equipment, an automatic spray traversing rig and exhaust booth were designed and fabricated. The booth and exhaust, Figure 9, were purchased but the traversing rig was designed at TRW. The traversing rig is composed of 1) variable speed motor, 2) a chain drive, 3) two guide rails with linear ball bushings attached to the spray head bracket and 4) limit switches to automatically stop and decelerate the traverse. Two spray heads were used to cover the panel width with a sufficient coating. The traverse speed can be controlled to 0 - 10 fps while the spray equipment variables are 1) air pressure, 2) spray liquid pressure and 3) spray pattern. The pattern was adjusted to an elongated, somewhat elliptical shape for best coverage. Each epoxy system requires a considerable familiarization period because of the difference in liquid viscosity and thinner or diluent characteristics.

Three epoxy formulations as follows were tried.

1. Bee Chemical Company

100 PBV D5H-30004 Epoxy Resin	50 PBV R-533 Thinner
100 PBV ET 438 Catalyst	50 PBV Butyl Cellosolve

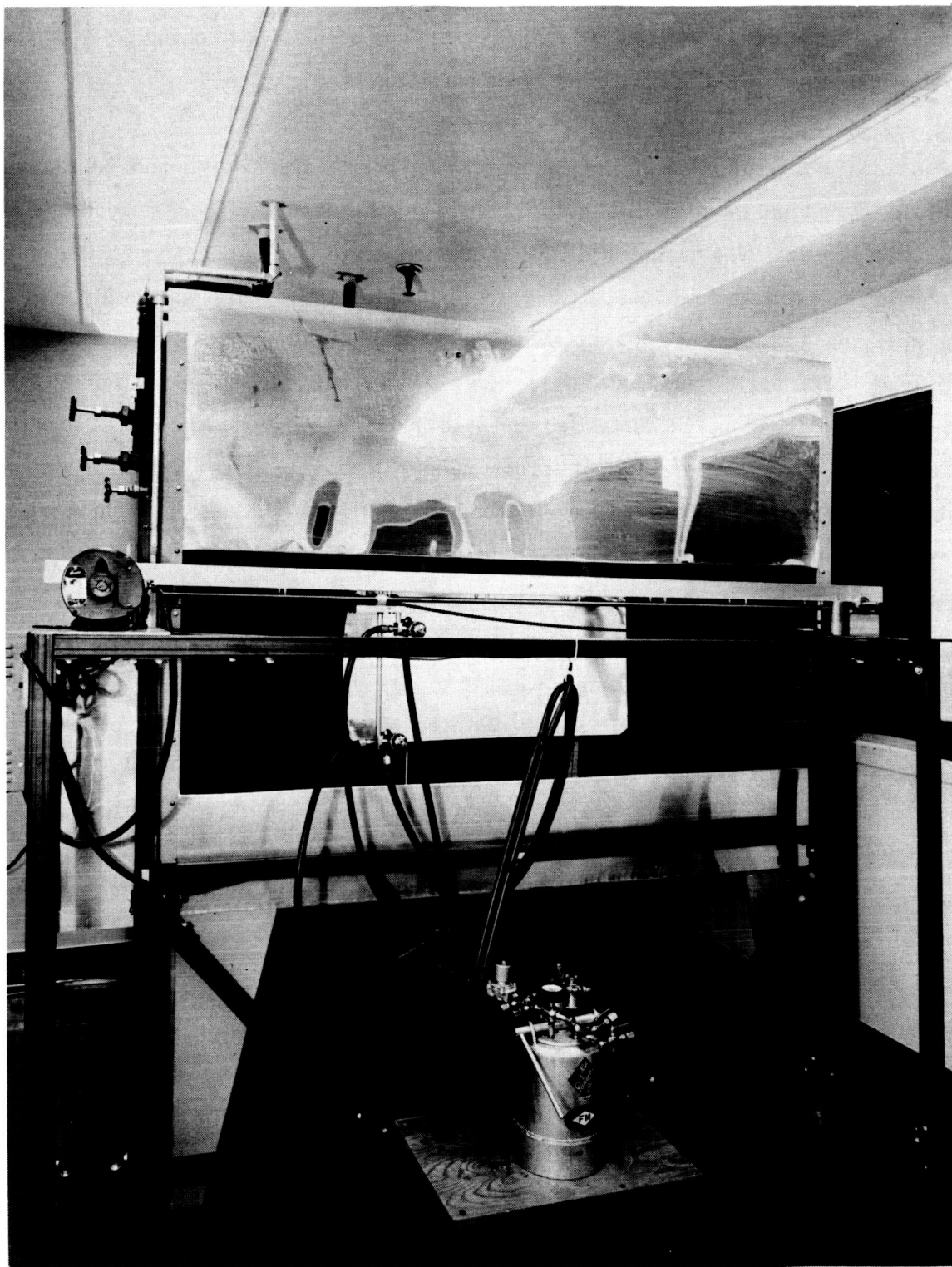
2. Emerson Cumming Company

Eccocoat EP 3	50 PBW of Part B Catalyst
100 PBW of Part A Epoxy Resin	15 PBW Diluent

3. Furane Inc.

Epocast 221  
100 PBW 221 Epoxy Resin  
8 PBW 9216 Hardener

All three formulations are 100% solids when cured out. In general, the first is a thinner formulation and results in a thinner film whereas the second and third are



SURFACE IMPROVEMENT COATING SPRAY AND EXHAUST EQUIPMENT

Figure 9

thicker and therefore result in a thicker film. Also, the thicker films require longer cure times. The success to which the three formulations were sprayed and cured are as ranked above, where the Bee formulation is best. The Bee formulation was not sufficiently thick (.0003 to .0005 inch; single coat) even in two or three applications to completely fill in the strain graininess. But the application was repeatable and uniform, indicating an adequate spray and traverse rig design. The exhaust system is also sufficient. The Emerson Cumming formulation resulted in a thicker coat (.001 to .002 inch). In one early case, a mirror-like coating was obtained. However, all other cases resulted in unacceptable coatings where various degrees of surface wrinkling were noted. The degree of wrinkling depth varied from about 0.1 or less to possibly 0.5 of the coating thickness itself. The condition was not due to film failure since the stock could be bent 180° in both directions without the layer crazing or separating. Since humidity, temperature and spray parameters were controlled, a major suspect is that the formulation requires improved mixing techniques. Possibly, spraying at higher than room temperature will also help in the thicker formulations. The third formulation was the least successful and tended to entrap air bubbles which did not drive off before curing. However, this formulation received the least attention and number of trial applications of the three.

The surface improvement process received a large share of effort during the study, and results indicate a more difficult developmental area than was previously anticipated. The fact that a mirror-like surface has been obtained with one formulation and that the spray process control is good in another formulation provides an indication that a solution is near.

The coating was applied to the panels prior to trimming which minimized any edge effects and allows some excess stock to handle without danger of damage. Prior to coating, the surface was wiped with acetone and immediately wiped with a dry lint-free towel. The panels were supported in contoured forms to prevent permanent surface distortion while being wiped. The Bee Chemical formulation with vacuum

evaporated aluminum and silicon oxide overcoats can be wiped with acetone or toluol without attack. The coating survived several hours submerged in acetone without visual degradation. Soft lint-free towels should be used however.

For the Bee formulation, the panels were heat cured in a specially built clean infra-red oven at 160° to 180°F for 2 hours prior to subsequent vacuum metallizing. The other two formulations require a longer period of about 4 to 6 hours for sufficient cure. Before the panels are placed in the oven, they are left in the room to allow the layer to become uniform. Dirt particles in the air were of concern until it was found that the panels did not collect particles in another area of the clean facility which was not being used by personnel. Since these areas belong to other groups during regular hours, it was necessary to spray at night or on weekends. This caused some schedule delays in itself.

### 3.2.6 Reflective Coating

The panels were vacuum metallized as listed in Table II prior to trimming. A silicon oxide coating was used between the epoxy and evaporated aluminum to improve the bond between the two. The outer layer of silicon oxide was provided as usual for protection during handling or cleaning.

Since the panels for this concentrator were not trimmed before aluminizing, it was necessary to coat three separate loads. This was due to the larger pieces being coated. A specimen from one of the trimmed-off pieces was measured for total directional and diffuse reflectivity over the wavelength range of 0.26 to 2.7 microns as shown in Figure 10. The total directional reflectance is 0.85. In previous phase 1 units this same value was 0.88 and 0.89; the latter is also shown in Figure 10. There are two significant differences between the phase 1 and 2 units as follows:

1. Phase 1 specimen ( $R = .89$ ) had 2200 Å silicon oxide and was on unstretched 5052-0 stock with an epoxy undercoat.
2. Phase 2 specimen ( $R = .85$ ) had 1300 Å silicon oxide and was on stretched 3003-0 stock with an epoxy undercoat.

TABLE II  
PERTINENT CONCENTRATOR FACTS

Weight

Shell and Joint Strips	5.58 lbs. *
Torus	5.28**
Brackets	0.32**
Adhesive and Cloth	<u>0.45**</u>
Total	11.62 lbs.

\*Calculated; \*\*Measured

0.59 lb./ft.<sup>2</sup> Intercepted Solar Flux

Materials

Shell; Aluminum Alloy	3003-D
Torus; Alum. Al.	1100-D
Brackets; Alum. Al.	6061-T6

Adhesive

Bondmaster M666 with Glass Fibre  
Cloth Cured at Room Temperature

Surface Coating

Bee Chemical Co. Epoxy .0003 - .0005" thick

Reflective Coating (Vacuum Evaporated)

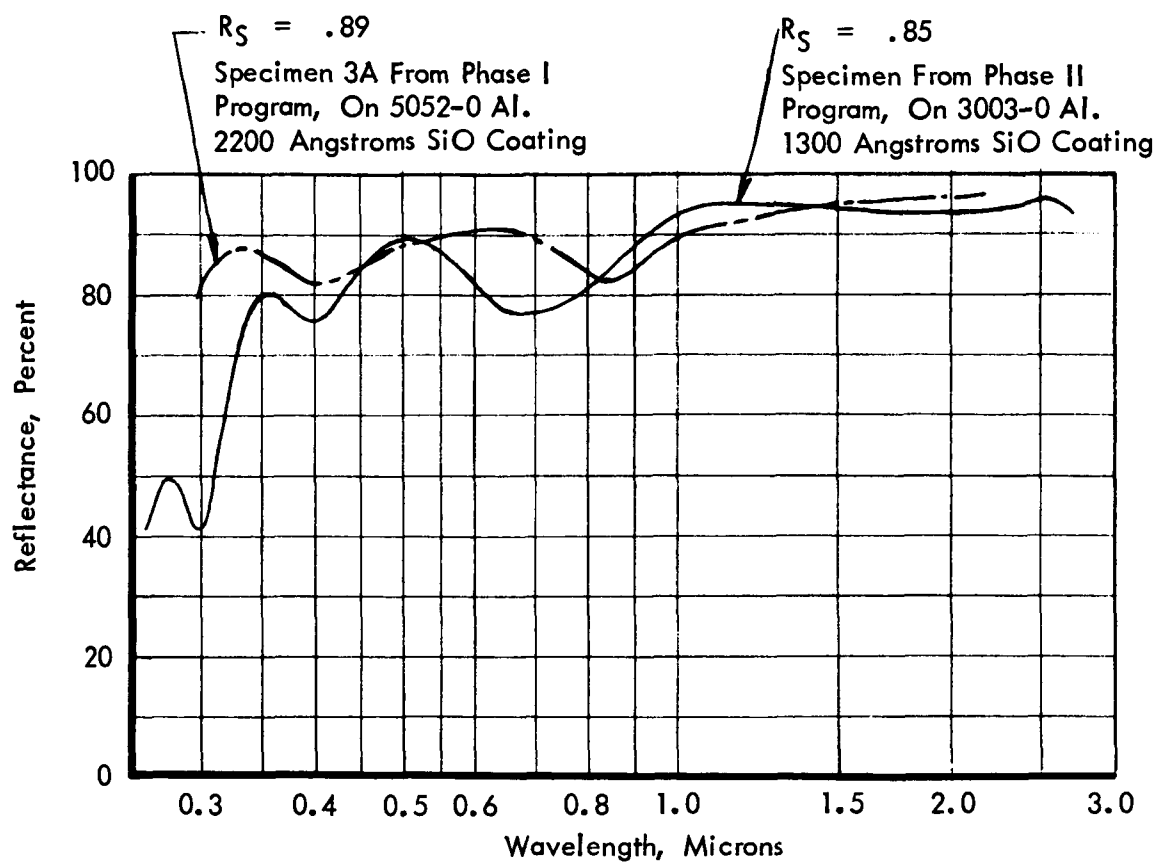
3100 Å Silicon Oxide Over Epoxy  
600 Å Aluminum (99.99% Pure)  
1300 Å Silicon Oxide Outer Layer

Reflectivity

0.85 Total to Solar Flux

Focal Length

25.6 Inches as Measured in Optical Inspection Rig



(Light Beam Incidence Angle -  
10° From Normal)

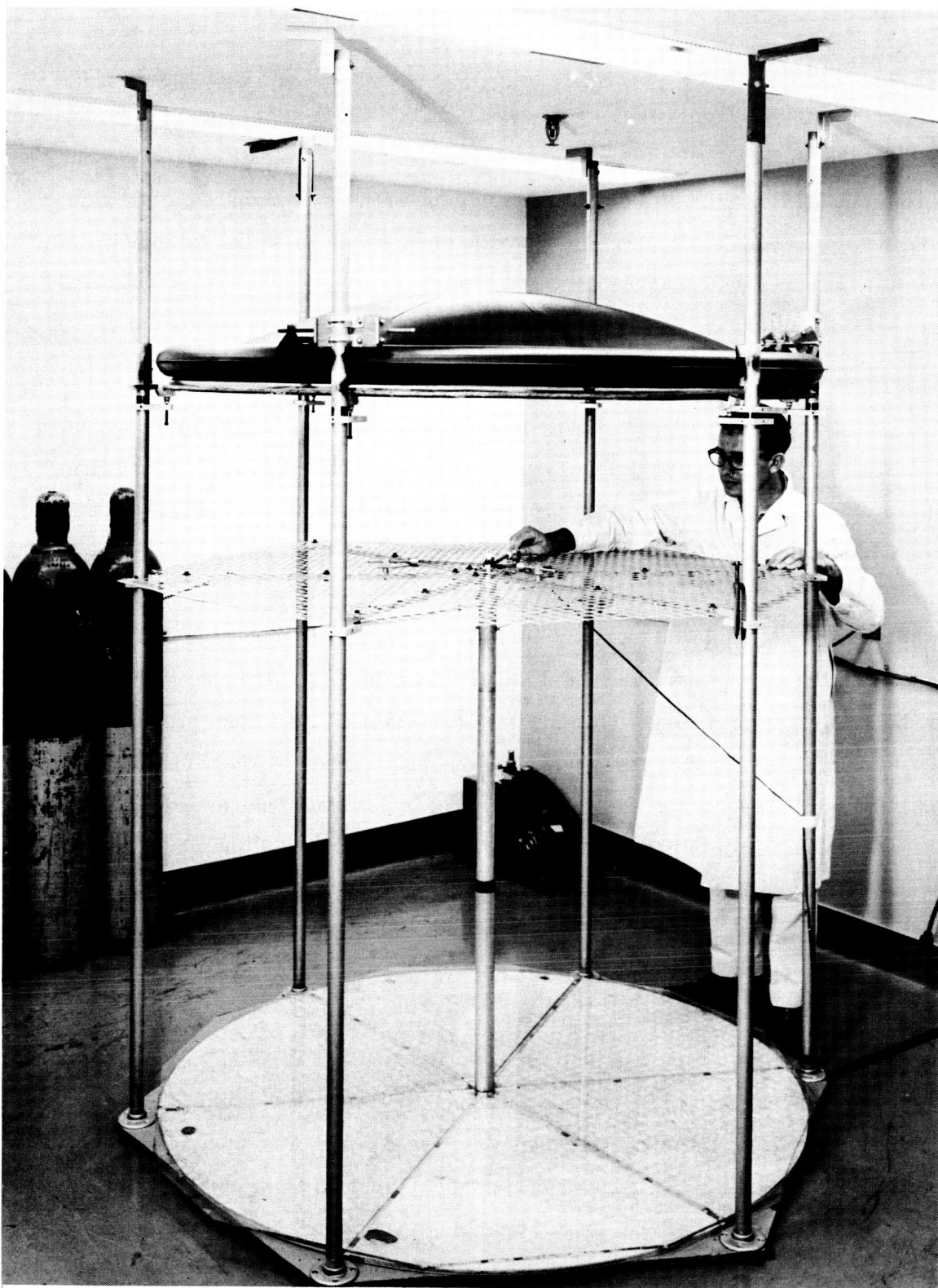
The phase 2 silicon oxide coat was reduced to 1300 Å to provide a peak at 0.5 micron where the solar spectrum peaks. This was achieved but there were some unwanted dips to either side of this value. The low reflectance in the ultraviolet range of 0.26 to 0.35 micron indicates that the silicon oxide layer may not have been optimum as regards oxidation proportions. A better silicon oxide layer would raise the reflectance values, especially at lower wavelengths.

### 3.2.7 Assembly-Shell

The significant change in the assembly procedure for this phase was in the use of the optical inspection rig upside down, Figure 11. Two advantages result 1) the glass meter can be aligned and observed throughout the assembly and 2) optical inspection records may be made at any point in the fabrication.

The silver was not removed from six small areas equally spaced on about a 55 inch diameter of the master surface. In all other areas the reflective coating on the sectors provided inspection of the stretched stock. However, the light must pass twice through the 0.6 inch thick master on its path to the grid and pattern. Except for the paraxial ray, these rays do not enter the glass at normal incidence. Thus, there is a refractive effect which can be 6.8 minutes of arc at the outside diameter if the glass has a 1.5 index of refraction. Not until the master is removed can absolute errors be measured. But, with the master in place a relative comparison between untrimmed stock, trimmed sectors and various phases during assembly may be made.

Optical inspection accuracy was also improved by making full scale photographs of the shadow and pattern. This was accomplished by tracing the grid pattern on a plexiglass sheet and placing photographic paper on 60° sectors which were placed underneath the plexiglass, Figure 11. Thus the pattern and shadow photograph on the paper. Figures 12a through 12f are one fourth reductions (approximately) of the full scale photographs for the final concentrator assembly, without glass master. Inspection photographs were taken at the following points during fabrication:



PROJECTED GRID OPTICAL INSPECTION RIG WITH GLASS MASTER  
AND ASSEMBLED CONCENTRATOR IN PLACE

Figure 11

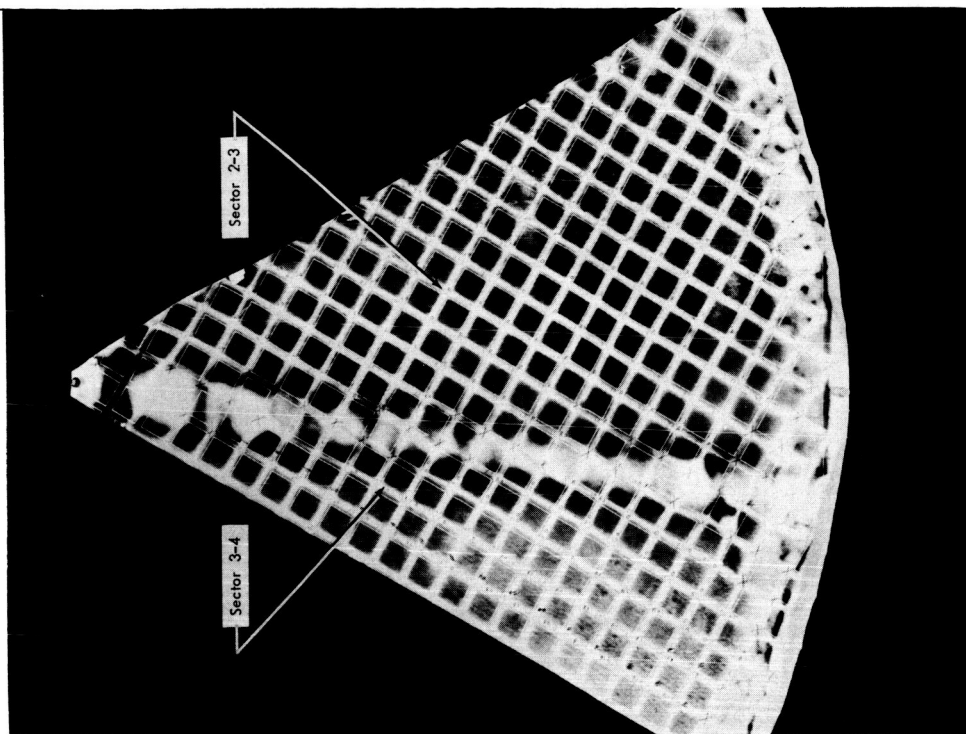


FIGURE 12b

SECTOR EDGE DISTORTION

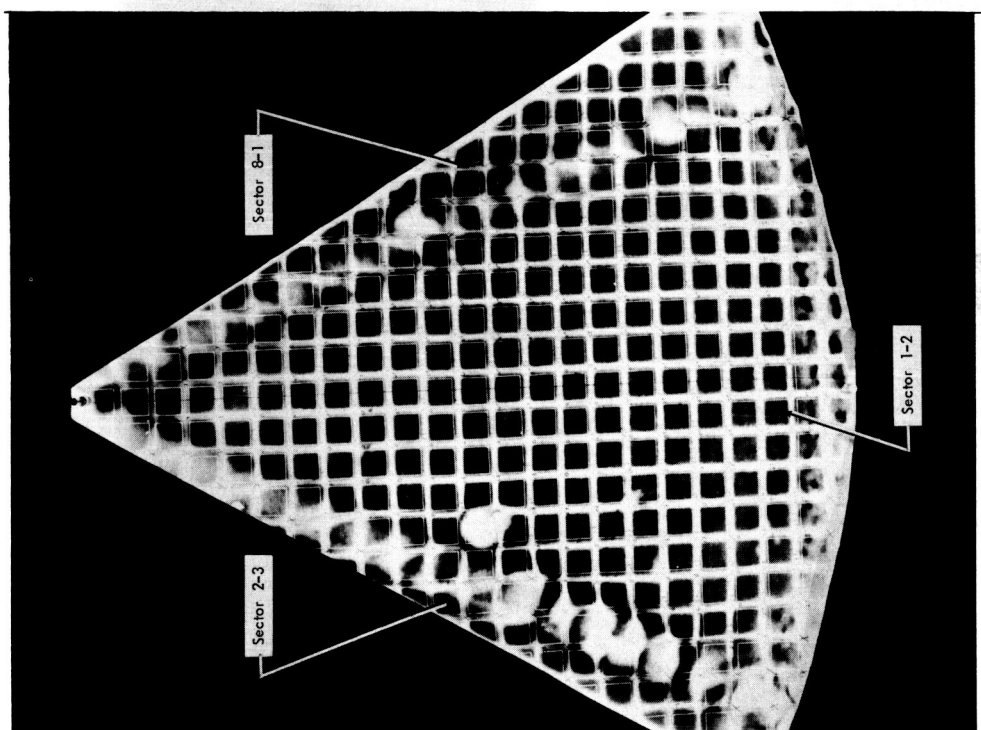


FIGURE 12a

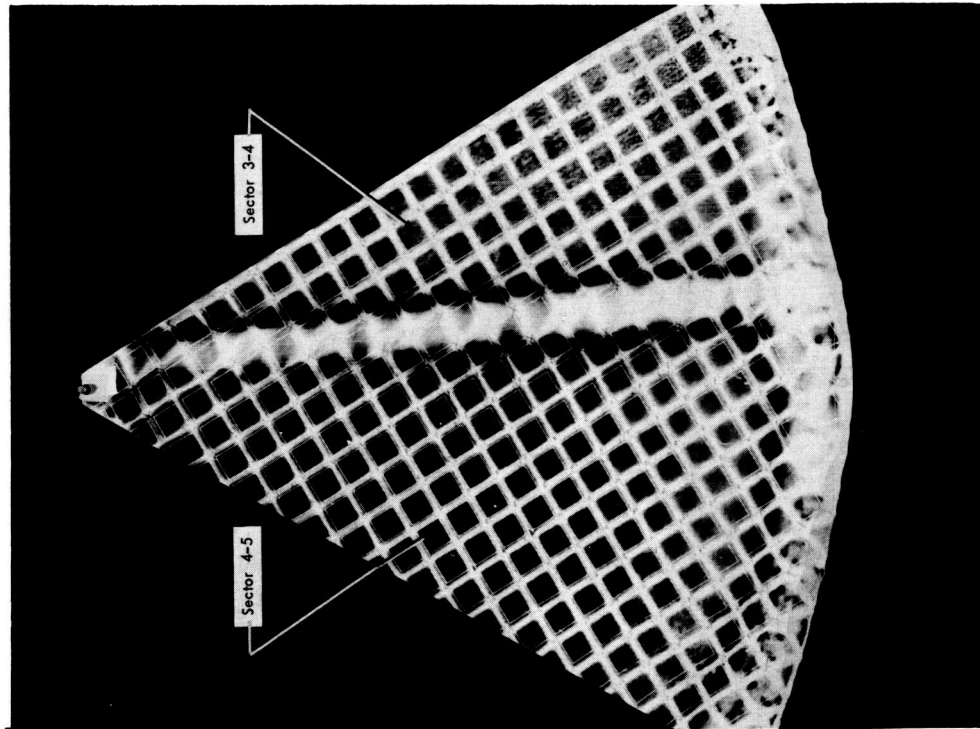


FIGURE 12c

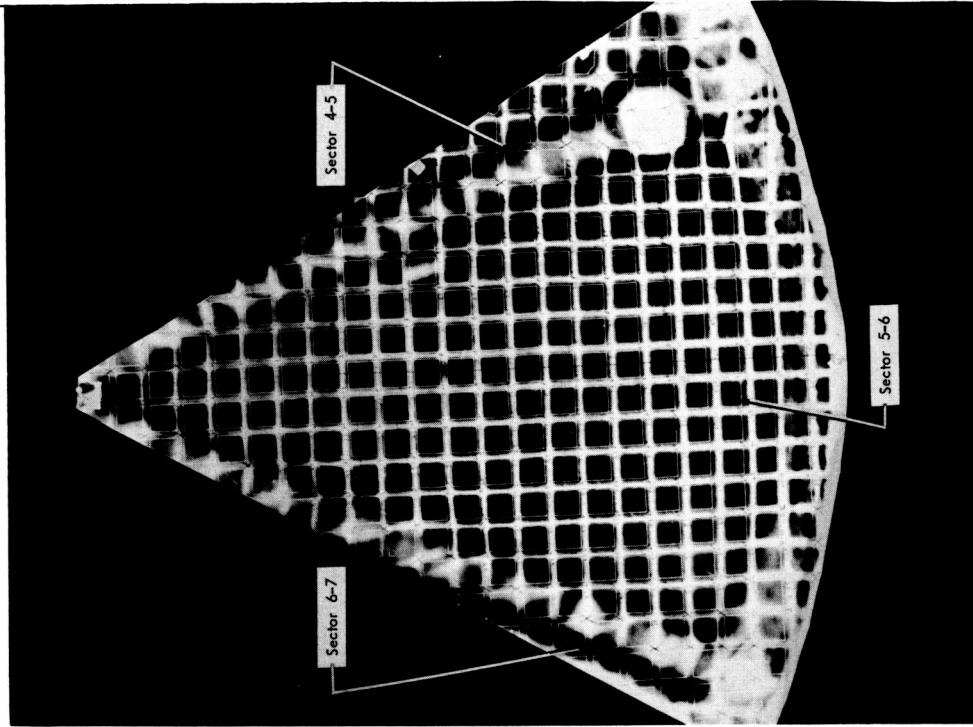


FIGURE 12d

SECTOR EDGE DISTORTION

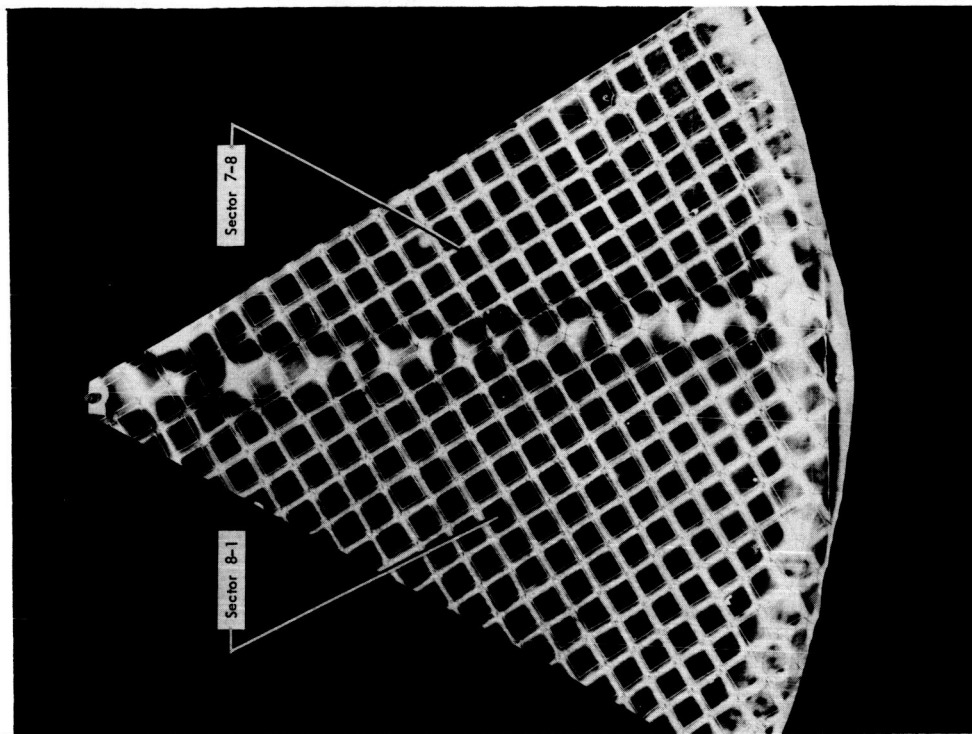


FIGURE 12f

SECTOR EDGE DISTORTION

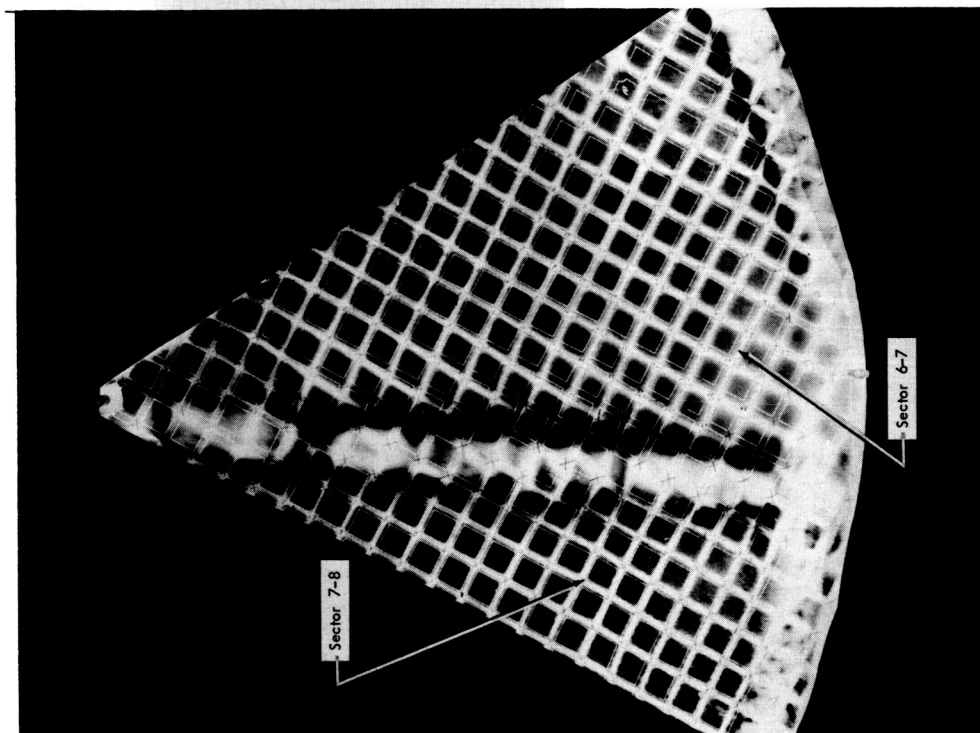


FIGURE 12e

1. Glass master with silvered convex surface. This provides evaluation of the master surface. Also at this point, the dial indicator setup used for inspecting the master on the stretch former was used. The run-out readings were plus or minus .004 inch and similar in cyclic nature as in Figure 8.
2. All 13 of aluminized stretched half panels before trimming. This evaluates the degree of conformance to the master.
3. All 13 of aluminized trimmed sectors. This evaluates the trimmed area only and the effect of trimming.
4. Best 8 sectors in place on tool, with radial joint strips in place, with vacuum bag on and with adhesive wet. This evaluates the bagged conformance of the sectors to the master.
5. Same as 4, but after cure. This evaluates the adhesive shrinkage effect on surface errors.
6. Same as 5, but without vacuum bag. This evaluates the unrestrained conformance of the cured shell to the master.
7. Cured shell and torus assembly. This evaluates the effect of bonding the torus to the shell.
8. Same as 7 but without the glass master in place. This provides an absolute measure of general surface errors.

The inspections at points 1 and 8 above were originally planned for the program. The intermediate checks were performed for use on the Brayton collector study, NAS 3-2789 (Lewis) and charged to that contract.

The glass master is supported at 6 points on the inspection-assembly rig and adjusted to shape with the screws at each location. Assembly was performed by standing on 6 wooden benches specially made for the rig.

During the trimming of sectors and inspection on the rig it became apparent that the radial edges showed a distortion such that the edges curved inward as shown in Figure 13a. Some sectors were trimmed from the opposite side, but there was the same distortion inward. Thus, the distortion appears due to a stress relief rather than trimming distortion. In the phase 1 program, this distortion went undetected because intermediate optical checks could not be performed. When distortion was measured on the final assembly, the reason was given solely as an adhesive shrinkage effect. This was logical based on similar experience with adhesive effects on the Sunflower program. However, there can be distortion due to both. Because adhesive shrinkage was originally considered to be the primary reason for joint distortion, a survey of adhesives was made in order to minimize the effect. Table III lists the formulations investigated. In general, an adhesive was chosen for low shrinkage and/or low modulus of elasticity. Of the formulations, the first five were chosen for final evaluation after radial joint specimens were prepared and inspected. Of these five, the first two were chosen based on minimum distortion and high bond strength.

Subsequent to the choice of adhesives with low distortion effects, the apparent stress relief condition was observed and a modification to the fabrication procedure was required. The distortion was now attributed to adhesive properties and/or the trimming effect. To reduce the inward distortion (Figure 13a) a strip of tape was placed on the tool (Figure 13b) and the sector joint was made directly over it. When the joint is vacuum bagged, the sector edge is forced to deflect away from the master during cure. As the vacuum bag is removed, the sector edge will partially return to its original shape. Three tape thicknesses of .0025, .005 and .006 inch were used, and the optimum thickness appeared to be between .0025 and .005. This thickness could not be obtained and the .005 thickness was used. However, the final joints on the 60 inch unit were over-compensated resulting in too much distortion in the opposite direction. Further work is required to optimize the joint design.

At this time, the need for a flexible adhesive was questioned, although low shrinkage is still considered desirable. Therefore, radial joints were prepared with the first

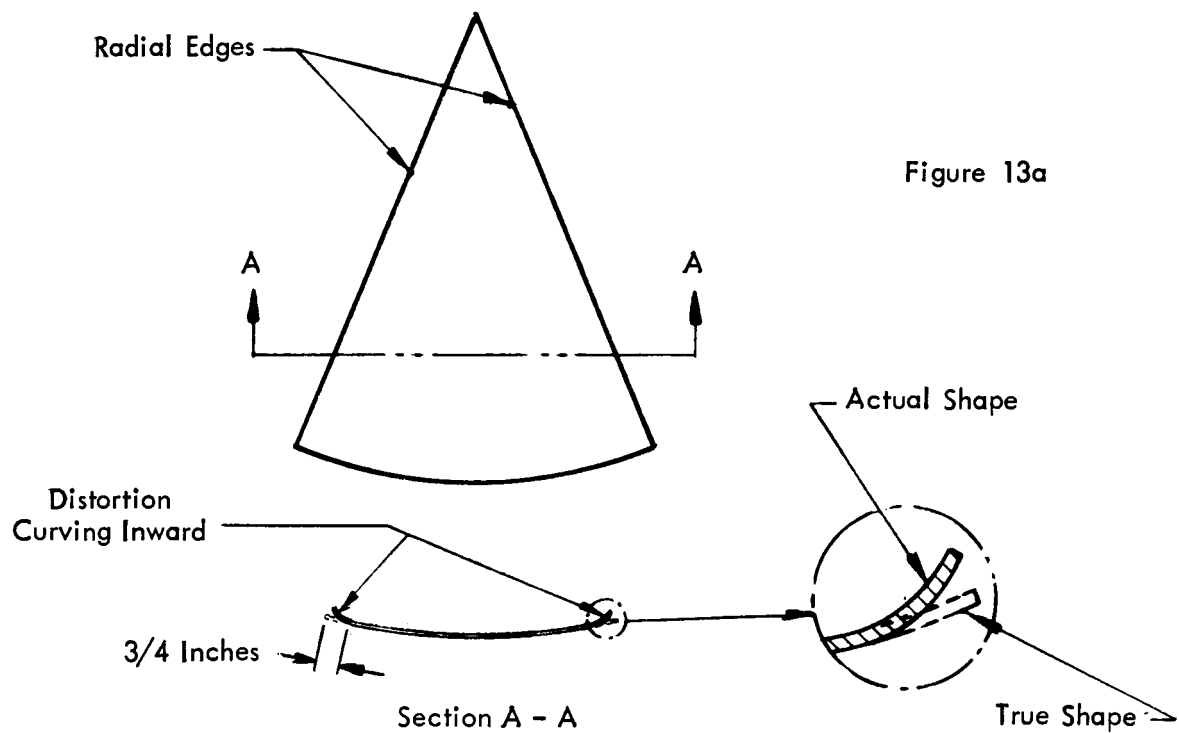


Figure 13b

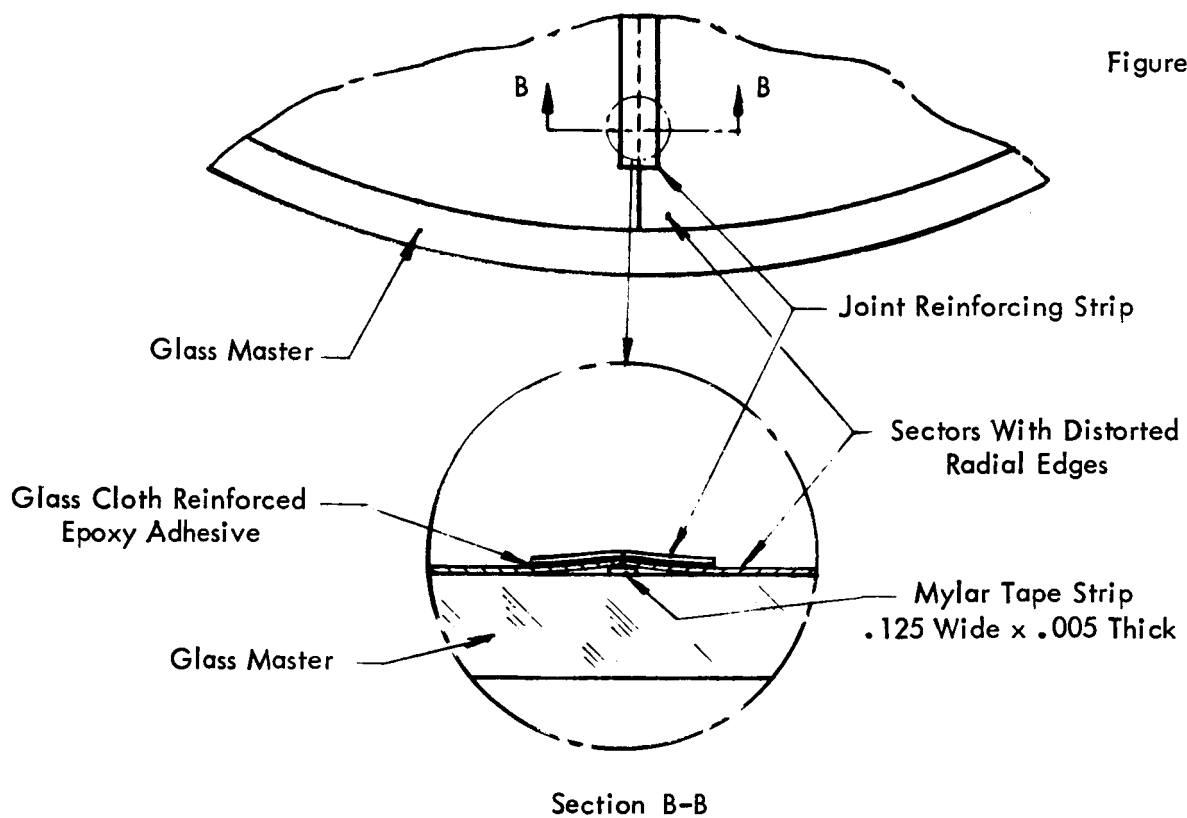


Figure 13

TABLE III

## ADHESIVES

No.	Resin	Hardener	Type	Manufacturer
1	Bondmaster M666-A	M666-B	Medium Syrup	Pittsburgh Plate Glass
2	Cepox 402	402 Hardener	Heavy Syrup	Chem. Development
3	Eccobond 45 LV	Cat. 15LV	Medium Syrup	Emerson and Cuming
4	Eccobond 285	Cat. 9	Thixo- tropic	Emerson and Cuming
5	Epon 921-A	921-B	Thixo- tropic	Shell Chemical
6	Araldite 6010	Versamid 125	Light Syrup	Ciba and General Mills
7	ERL 2774	Versamid 125	Light Syrup	Union Carbide and General Mills
8	ERL 2774	ZZL-0822	Light Syrup	Union Carbide
9	EPON 919-A	919-B	Heavy Syrup	Shell Chemical
10	Araldite 6010	Polyamide 825	Light Syrup	CIBA
11	Bondmaster M777-A	M-777-B	Thixo- tropic	Pittsburgh Plate Glass
12	Bondmaster M648-T	Cat. CH-9	Heavy Syrup	Pittsburgh Plate Glass
13	Eccobond Aluminum-A	Aluminum-B	Heavy Paste	Emerson and Cuming

two adhesives in Table III and Bondmaster M666 which is a more rigid epoxy and was used in previous phase 1 units. The M666 joints appeared to have less distortion and was therefore chosen for the final assembly. The conclusion is therefore that the inherent distortion of the trimmed edge is the primary cause of distortion in the assembly, and adhesive properties cause secondary effects.

The radial joints were bonded with .004 inch thick glass fiber cloth reinforced adhesive. The methods of applying the adhesive to the joint strips and the vacuum bag were the same as in the phase 1 work.

### 3.2.8 Assembly-Torus

The torus assembly proceeded without difficulty. Bondmaster M666 was also used to bond the torus halves together. A .010 inch thick glass fiber reinforcing cloth was used. To assure conformance of torus shape to shell shape, the outer torus half was loaded with sand bags during cure. There was no measurable distortion of the glass master due to the added weight. Also, the torus after cure conformed to the shell shape.

### 3.2.9 Assembly-Concentrator

Bondmaster M666 with .010 inch glass cloth was used for the bond between the torus and shell. Some weights were used to force the adhesive to fill any voids that might exist. However, the weights were minimized, since this could locally distort the torus, and result in a distortion upon release. Adhesive was minimized to avoid filletting and the possibility of mark-off. The degree of torus-to-shell bond mark-off was slight when inspected.

The 3 mounting brackets were also bonded to the torus with .010 inch thick glass cloth reinforced Bondmaster M666. Eight rivets per bracket (Figure 5) were also used for attachment. The rivets were put in while the adhesive was still wet and therefore provided restraint during curing. They also insure against a possible total bracket separation should a local separation propagate.

Prior to removal of the glass master for inspection of absolute surface errors, the concentrator was rigidly fastened to the inspection rig via adapters between the 3 mounting brackets and the poles (Figure 11). The master was then lowered, placed on edge and removed from the rig. Thus the concentrator remained in the same position and was optically inspected while mounted upside down at the 3 mounting positions. Thus a 1 g load was sustained during inspection.

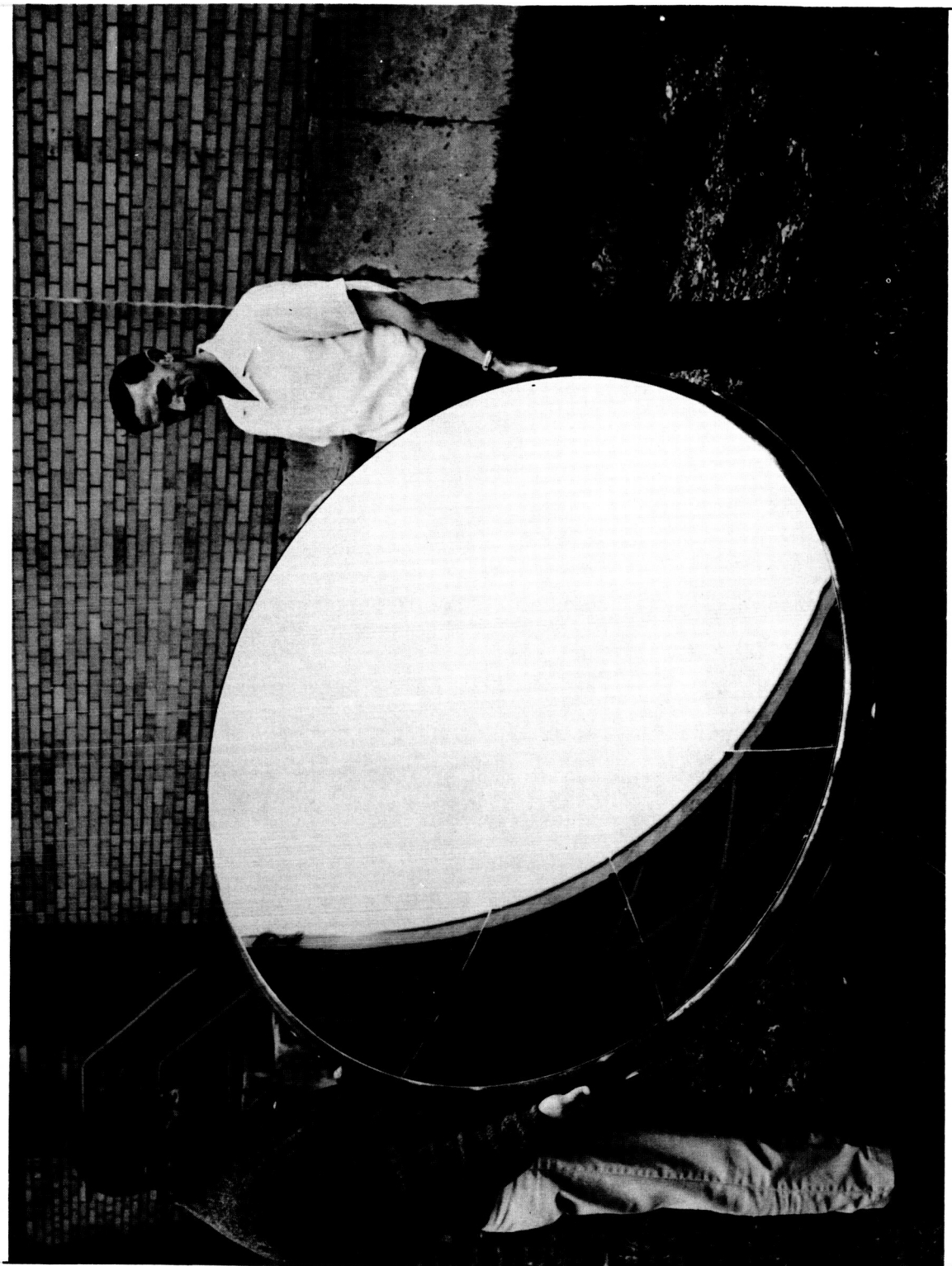
Front and back views of the 60 inch concentrator are shown in Figures 14 and 15, respectively.

### 3.3 Inspection

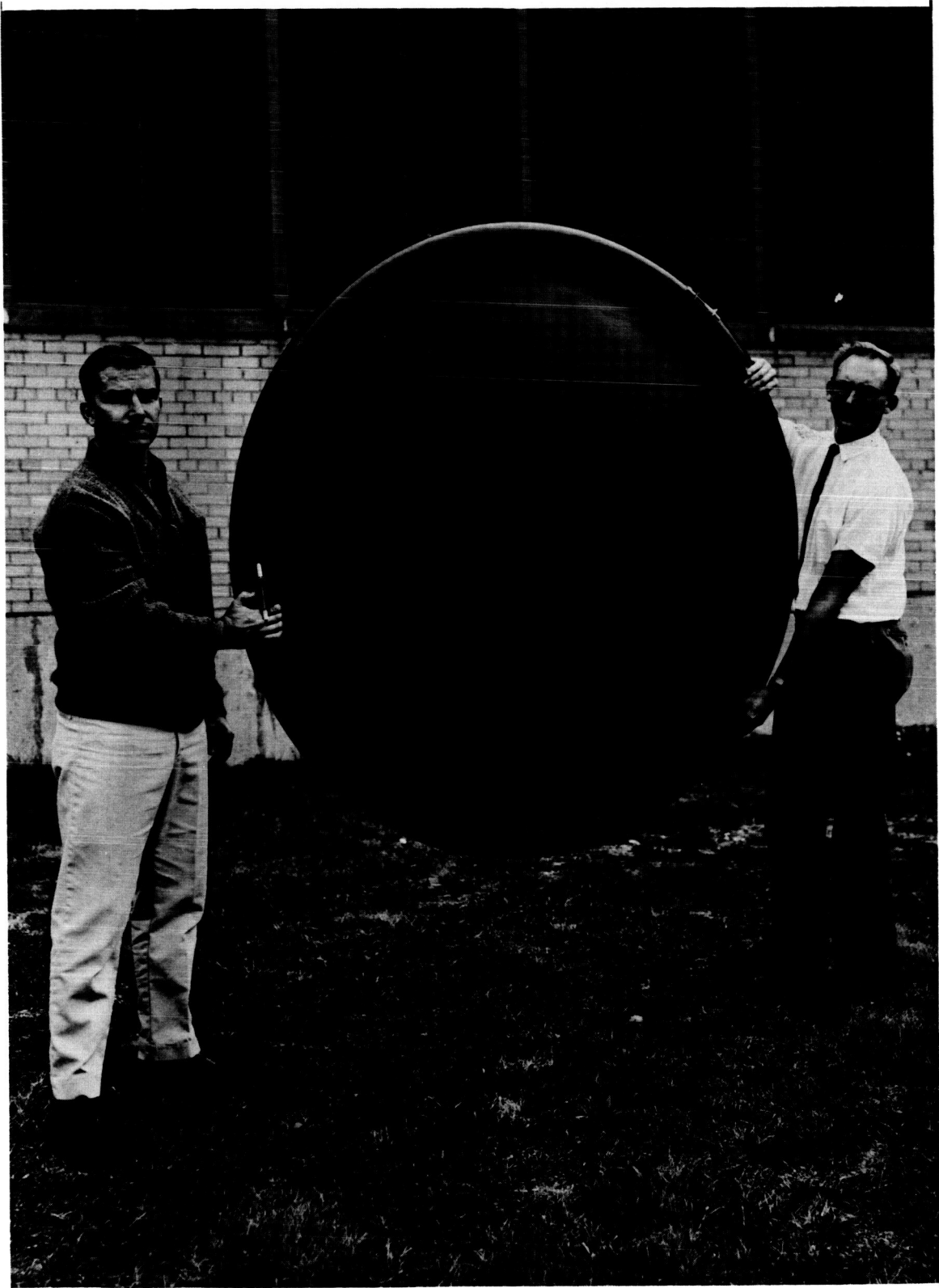
#### 3.3.1 Optical

The master was inspected by dial indicator and the projected grid optical method. The dial indicator results (Figure 8) showed that circumferential surface errors did not exceed 0.9 minute arc. As can be seen from the run-out patterns for the 4 different circumferential measurements, the radial surface errors are not large. This is also substantiated by the optical inspection photos, although absolute errors could not be measured because of the glass master refraction effect. No attempt was made to correct for the refraction because the composition of the glass master, and therefore the index of refraction, is not known. For a variation of 1.45 to 1.70 in refractive index (range for glasses) the ray deviation at the outside edge would vary from 6 to 12 minutes. This difference is greater than the errors to be measured. Measurement of the errors along a radial trace (parabolic curve) requires a more complex method of inspection involving coordinate point and waviness measurements and was not attempted.

If the circumferential error data is cross plotted to obtain run-out versus radial position for various angular stations, then a maximum error of 2.1 minutes is obtained. The maximum radial and circumferential errors are in the same region of the master. Thus a maximum resultant error of 2.3 is conceivable. From this data it is apparent that master errors are near 2 minutes maximum.



SOLAR CONCENTRATOR - FRONT VIEW



SOLAR CONCENTRATOR - BACK VIEW

Figure 15

The projected grid inspection photographs of the final concentrator are shown in Figure 12a - f (at approximately 1/4 scale). These were taken with the master removed and can therefore be used to establish error probability curves and to predict performance. The data was reduced separately by sectors and as a total effect. There were differences in the probability curves from one sector to another as is shown in Figure 16 a and 16b. Errors for the entire concentrator are shown in Figure 16c. These errors are absolute. If the errors are measured as x and y components over the projected grid screen pattern, the curves in Figure 17 result. Note the tendency for fewer errors near zero in Figure 16 but a predominance near zero in Figure 17. Since the errors in Figure 16 are absolute this would be expected. Note also that sector 6-7 has a considerably different curve than the others. When the shell was being assembled, it was noted that this sector was away from the master surface in some areas when finger-tapped. It was not removed since it was expected to conform during and even after vacuum bagging and cure. This was not the case and the exact cause of error is not known. It could be due to 1) too large a sector angle resulting in butting at the radial joints or 2) a distorted sector. The first case is more likely the reason. The errors measured here are of the general surface contour and do not include such errors as are caused by surface finish, small surface imperfections such as dents and radial joint deviations within plus or minus 1/2 inch of the joint. However, the general shape is the most important factor in determining the concentration ratio of a specific concentrator design.

The errors measured have been reduced by a factor of over 2 to 1 including sector 6-7 and by a factor of 4 to 1 excluding it when compared with the phase 1 work. Both the absolute and x and y component error curves approximate closely a normal distribution curve. However the curve of absolute values show zero probability at zero surface error which can be shown mathematically by constructing a curve from the x and y component data. The x and y component error curves can be used to predict performance by comparison with a mathematical analysis (Reference 4) which uses a normal distribution curve model for radial and circumferential components. To provide the most useful data for such an analysis, however, it would be desirable to have a grid made on a polar coordinate basis.

ABSOLUTE SURFACE SLOPE ERRORS  
ASSEMBLED CONCENTRATOR

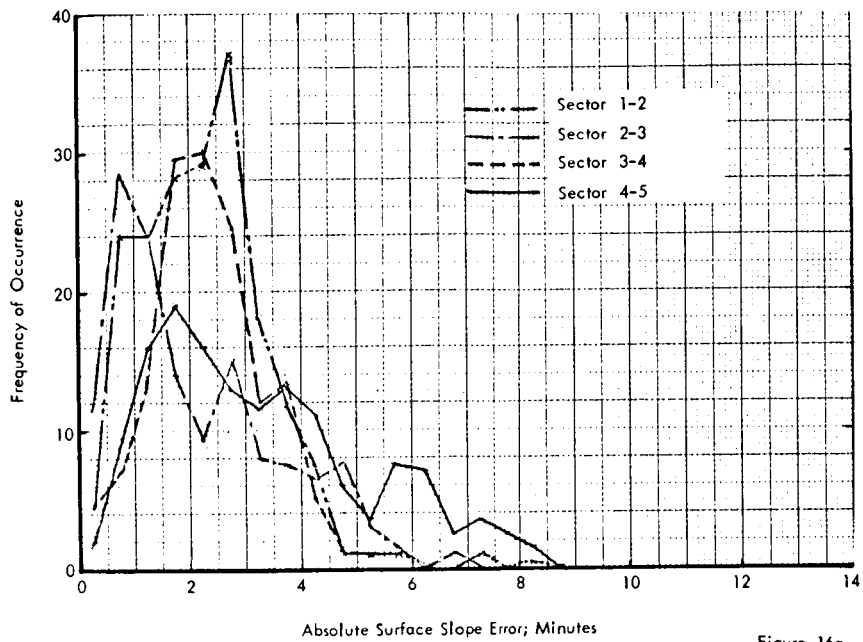


Figure 16a

ABSOLUTE SURFACE SLOPE ERRORS -  
ASSEMBLED CONCENTRATOR

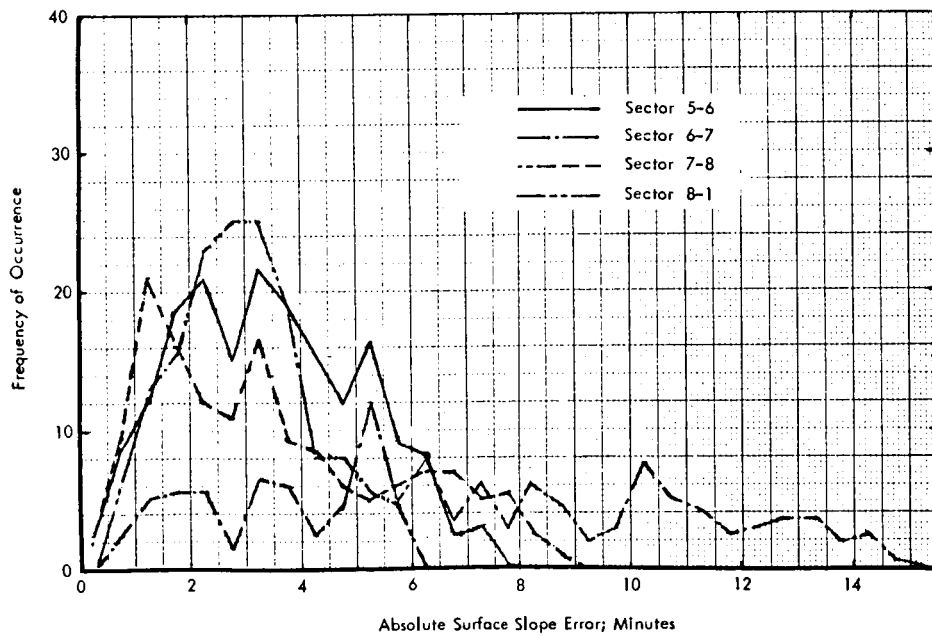


Figure 16b

# ABSOLUTE SURFACE SLOPE ERRORS ASSEMBLED CONCENTRATOR

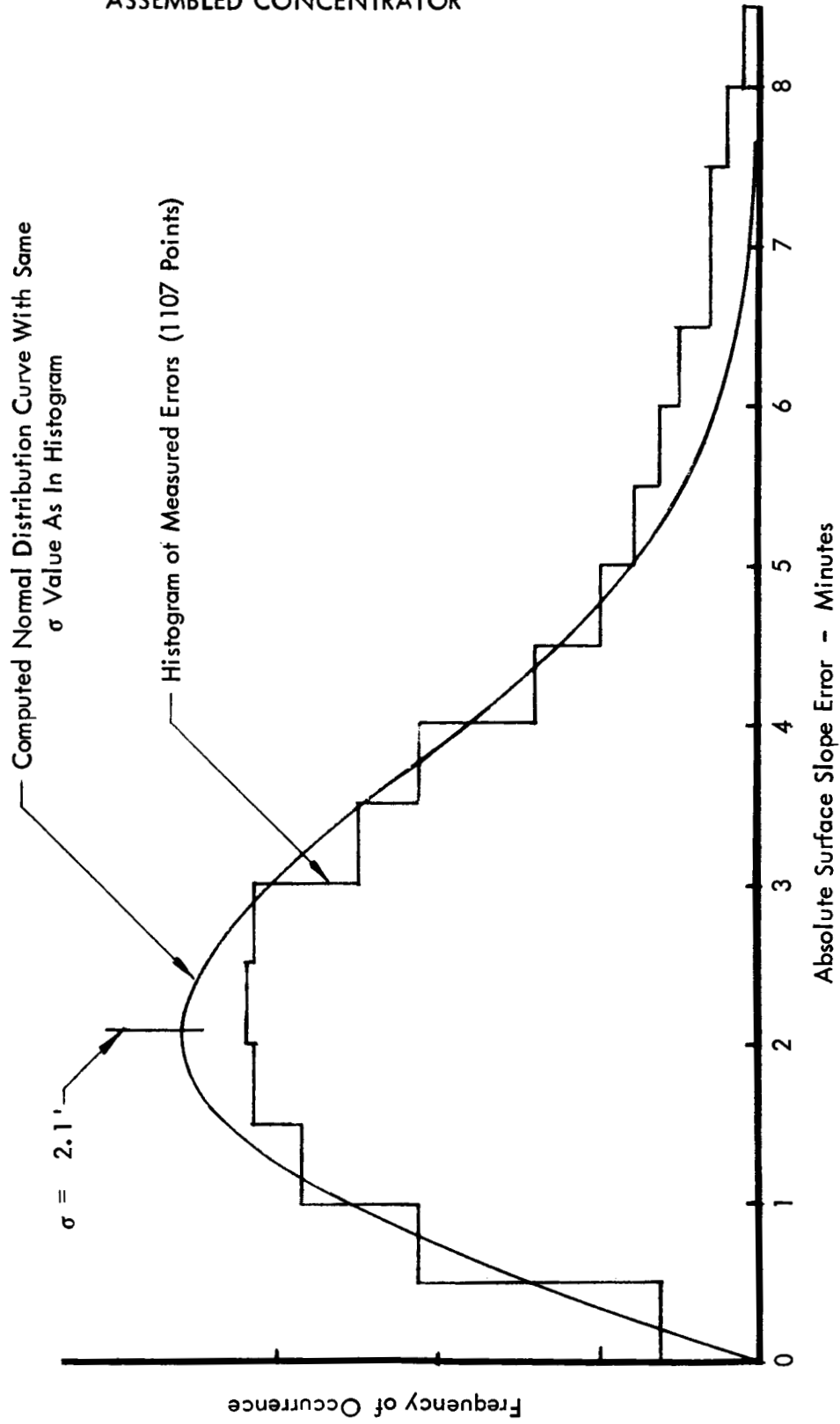
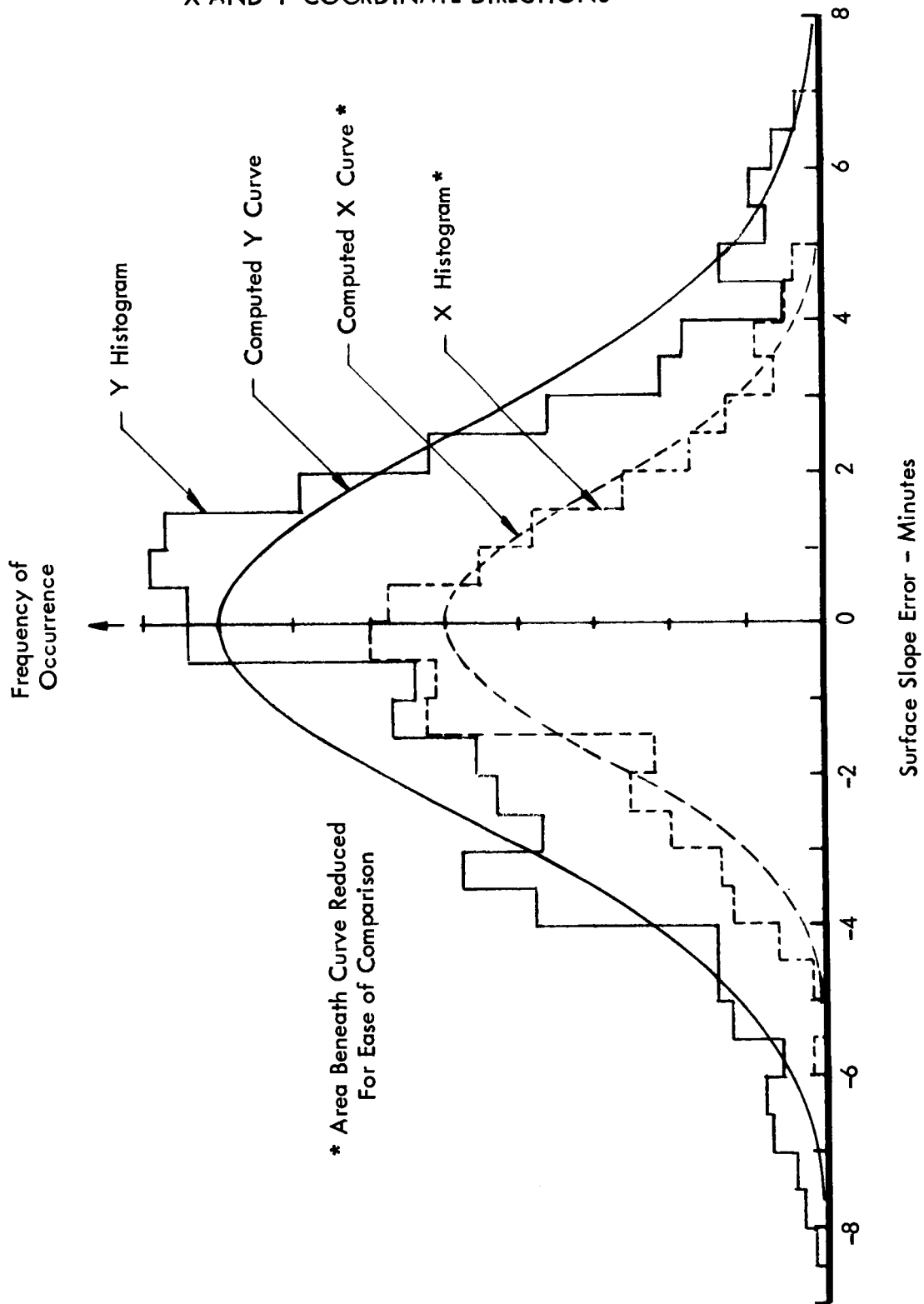


Figure 16c

# DISTRIBUTION OF SURFACE SLOPE ERRORS IN X AND Y COORDINATE DIRECTIONS



Inspection photographs taken at several steps during fabrication have revealed several facts. Figure 18 shows the absolute errors measured on sector 5-6 before and after trimming; and the glass master surface over which sector 5-6 was placed for inspection. These errors contain a refraction error due to the incident light passing through the glass master twice. However, relative comparisons can be made. The tool errors are lower than for the sector as can be seen by comparing the one  $\sigma$  and maximum error values. The one  $\sigma$  values vary by about 0.8-0.9 minute and the maximum values vary by about 1.5 to 2.0 minutes. A comparison between the untrimmed and trimmed stock shows only a small change in error distribution. The increase in the one  $\sigma$  value after trimming is probably due to the stress release distortion which occurs at the radial edges. It should be noted (Figure 18) however, that the measured curve (shaded for clarity) does not match the calculated curve for the tool as well as do the other two pairs. In comparison, the measured curves are more closely matched for the three cases than are the computed curves.

When the trimmed sectors were placed side by side on the tool and inspected, a dark strip was noted where the edge errors should have occurred. This indicated the surface distortion due to stress release after trimming. An approximate value for the maximum slope due to this distortion is 15 minutes based on the width of the shadow and distance between the grid and pattern. This error was reduced when the mylar strips were used during shell assembly (Section 3.2.7).

The grid was spaced 50 inches from the pattern and a 1 minute surface error would displace the projected shadow by .029 inch. The errors can then be read to the nearest 1/2 minute, or at most, the nearest minute depending on the local surface finish.

### 3.3.2 Weight

The weight breakdown for this unit is shown in Table II and totals 11.6 pounds or 0.59 pounds/ft<sup>2</sup> of intercepted solar flux area.

# ERROR DISTRIBUTION CURVE

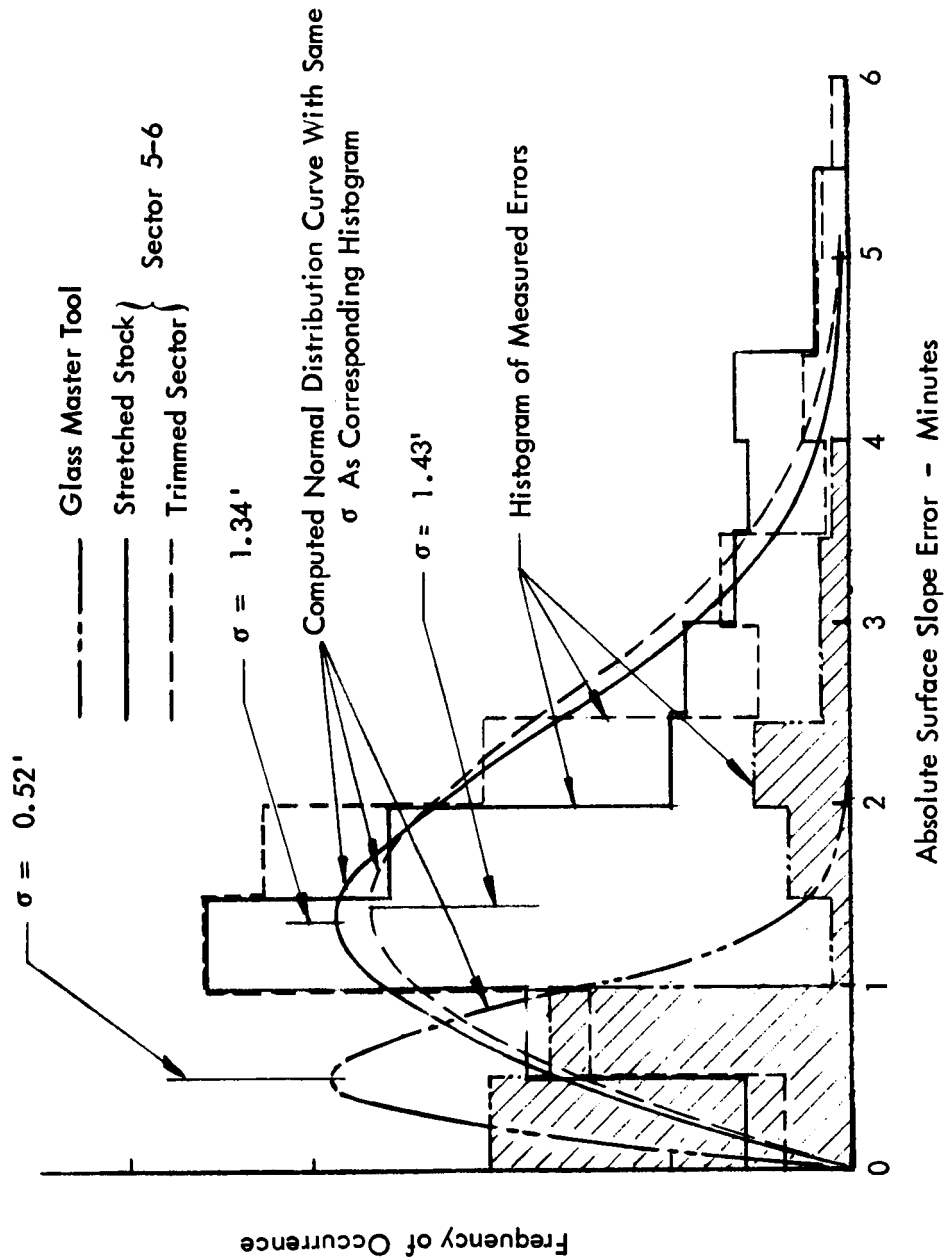


Figure 18

### 3.4 Predicted Performance

It is difficult to predict precisely what the efficiency versus concentration ratio curve would be with just the general surface slope errors. The surface graininess alone will account for a measurable degradation effect, which is further added to by sector 6-7 and radial joint errors. A qualitative comparison between phase 1 and phase 2 concentrators is shown in Figure 19. The phase 1 unit has shown good efficiency values for the 1000 to 3000 concentration ratio range. Based on the improved general surface, the phase 2 unit is expected to appear as in curve 2.

Curve 2 will cross over curve 1 because of the lower reflectivity value and greater percentage of strain graininess on the phase 2 unit. However, the efficiency will fall off much more slowly with increasing concentration ratio.

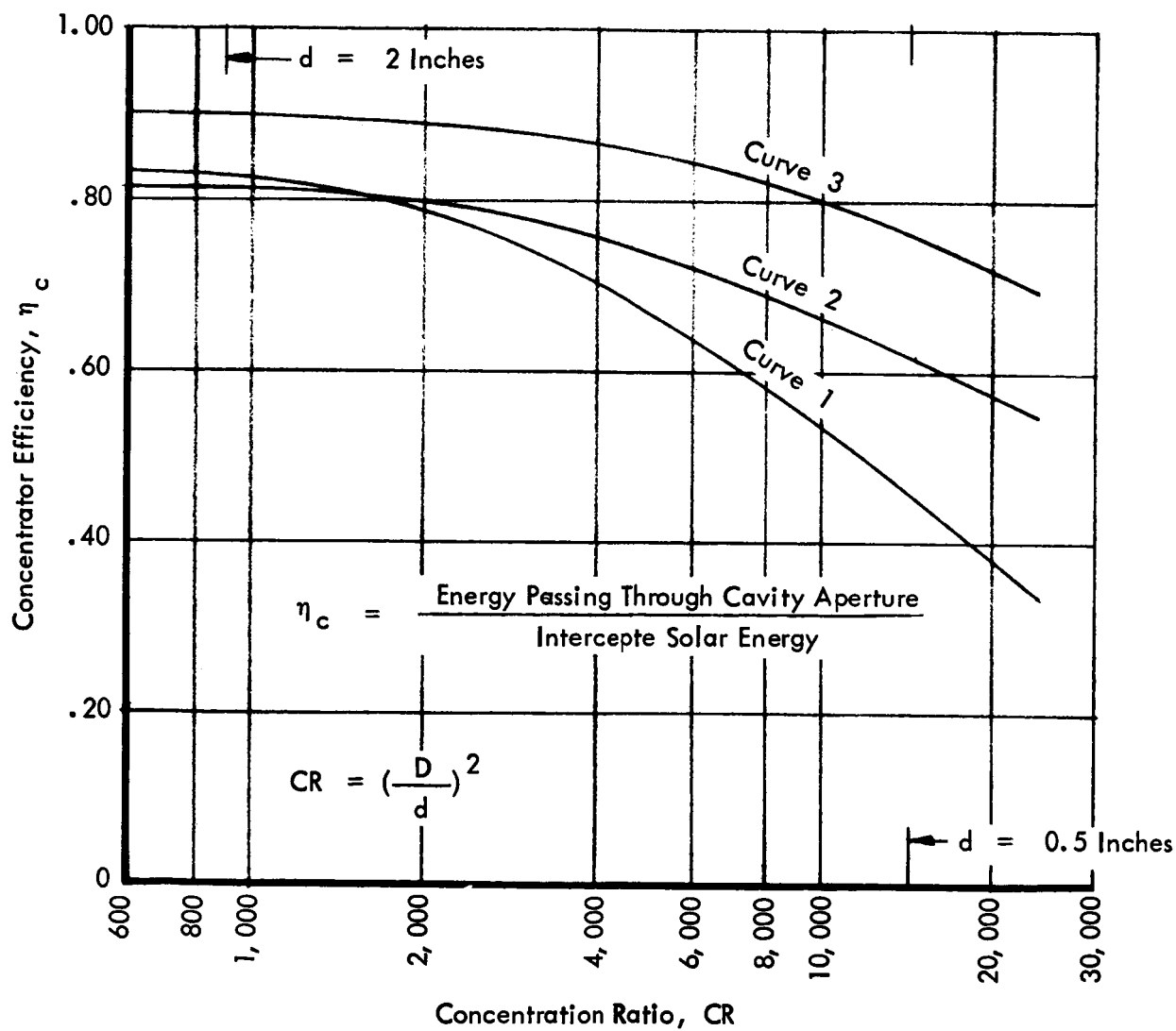
Curve 3 shows the predicted performance with improved surface finish, joints and reflectivity. Such a unit would have higher efficiency values in the 4000 to 10,000 concentration ratio range. The effect of sector 6-7 and the joint errors could be eliminated in solar calorimeter testing by masking out those areas.

# CONCENTRATOR EFFICIENCY VERSUS CONCENTRATION RATIO

Curve 1, Phase 1 Concentrator

Curve 2, Phase 2 Concentrator

Curve 3, Design Goal



#### 4.0 CONCLUSIONS AND RECOMMENDATIONS

Based on the results of this phase 2 work, the following conclusions and recommendations have been listed:

1. The glass master has surface slope errors of about 2 minutes maximum and is sufficient for the quality of concentrators required by the design specification.
2. Aluminum alloy 3003-0 has superior strain properties for the stretch forming process, although surface graininess is more pronounced than in the 5052-0 aluminum alloy.
3. The surface errors observed at the radial joints of the phase 1 units are caused primarily by a stress relief due to trimming. Adhesive shrinkage is a secondary factor in causing surface distortion at the joint.
4. A torus reinforcing member attached directly to the shell is the preferred configuration for the known environmental loads and thermal conditions.
5. Additional improvements in specific areas will further improve the concentrator performance. However, an improvement in general shape alone was the major improvement factor required of the phase 1 design. The improvement has been demonstrated in this phase 2 work wherein surface errors of 8 minutes or less were measured.
6. A thicker surface improvement coating is required to mask the strain graininess resulting from stretch forming. Several samples of a thicker epoxy coat with a mirror-like finish were prepared during this phase. However, the process control did not allow repeatability and a thinner epoxy coating was used on the unit. Uniform application and repeatability by the spray equipment was demonstrated using the thinner epoxy. Additional work is required in application of thicker coats.

7. A phase 3 program is recommended wherein the two major tasks would be to:

- a. Develop the application of a thicker surface improvement coating.
- b. Develop a method of minimizing radial joint errors.

Following the successful performance of these two tasks a phase 3 unit would be fabricated and delivered for solar evaluation.

## REFERENCES

1. von Karman and Tsien, "Buckling of Spherical Shell by External Pressure", International Aero Science, V7, N2, pp 43-50, December 39, pp 556-560.
2. Reiss, E. L. "Axially Symmetric Buckling of Shallow Spherical Shells Under External Pressure, ASME Trans, V80, 1958.
3. ER 5048, "Final Report - Fabrication of a 60 Inch Diameter Stretch Formed Aluminum Solar Concentrator," September 1962, NASA Contract NAS 7-154.
4. Shrenk, G. L. , "Theoretical Analysis of Solar Reflectors", Report 3193, Allison Division of GM, July 1963.

## SYMBOLS

$c$	=	Specific heat; BTU/lb-hr
$D$	=	Concentrator diameter, in.
$d$	=	Cavity aperture diameter, in.
$E$	=	Modulus of elasticity; psi
$g$	=	Inertia load
$h$	=	Shell thickness, in.
$M$	=	Mass; lbs.
$(N_{\theta})_p$	=	Circumferential membrane force; lb./in.
$(N_{\phi})_p$	=	Meridional membrane force; lb./in.
$(N_{\theta})_s$	=	Circumferential membrane force; lb./in.
$(N_{\phi})_s$	=	Meridional membrane force; lb./in.
$q_i$	=	Heat rate in; BTU/hr
$q_o$	=	Heat rate out; BTU/hr
$p$	=	Pressure load; psi
$p_{cr}$	=	Critical pressure; psi
$R$	=	Radius of curvature; inches
$T$	=	Temperature - °R
$t$	=	Time, minutes
$\alpha_s$	=	Absorptivity of solar flux
$\epsilon_t$	=	Emissivity of thermal radiation at concentrator temperature (300° to 600°R)
$\theta$	=	Orbit angle; degrees
$\mu$	=	Poisson's ratio
$\phi$	=	Angle between normal to shell surface and axis of revolution
$\eta_c$	=	Concentrator Efficiency